DEPARTMENT OF PHYSICS & ASTRONOMY

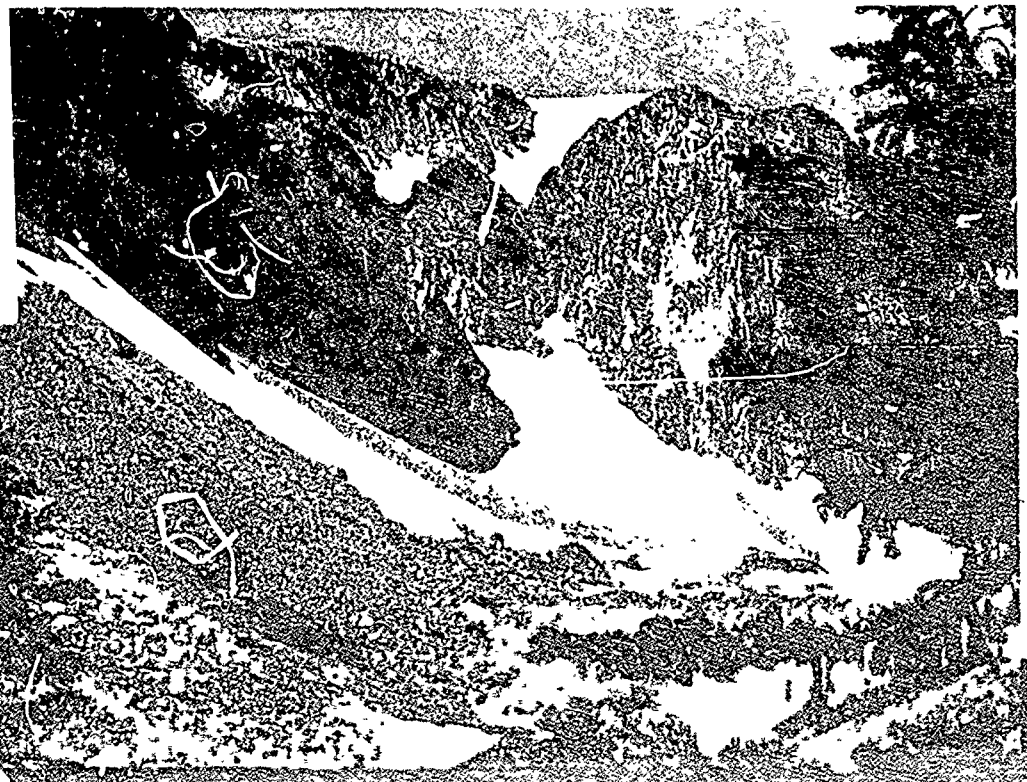

UNIVERSITY OF WYOMING

LEVEL II

12

FINAL REPORT

(6) DETERMINATION OF THE OPTICAL PROPERTIES OF HOLLOW GLASS SPHERE AEROSOLS.

NAVAL AIR SYSTEMS COMMAND
CONTRACT #(15) N00019-77-C-0262

FOR THE PERIOD

(9) APRIL 28, 1977 - JULY 28, 1978

Final rept. 28 Apr 77-28 Jul 78

DEPARTMENT OF PHYSICS AND ASTRONOMY
University of Wyoming
University Box 3905
Laramie, Wyoming 82071

(11) 28 Jul 78

(12) 42 p.

Prepared by:

(10) Todd A. Cerni
Research Associate

Approved by:

Theodore J. Pepin
Principal Investigator

407 537

1

I. Development of Optical Models

Optical modeling of hollow glass sphere aerosols was undertaken with a two stage approach. The first stage was to develop a model for homogeneous or solid spheres. This was a logical means of proceeding, since modeling of homogeneous spheres is by far the easier of the two tasks and is the area which has received by far the greatest attention from other investigators, hence providing copious examples with which to check our results. The homogeneous glass sphere model, based on the formulation of Mie (1908), was developed without any serious problems and was successfully tested against examples contained in Wickramasinghe (1973), Deirmendjian (1969) and Kuriyan et al. (1974).

Figures 1-5 depict a sample of the results obtained from the optical model for homogeneous spheres. The quantities which appear in Figures 1-5 and those pertinent to the optical model are

$$Q_{ext} = C_{ext}/\pi R^2. \quad (1)$$

$$Q_{ext} = Q_{scat} + Q_{abs}, \quad (2)$$

$$Q_{ext} = Q_{ext}(m,x), \quad (3)$$

$$x = 2\pi R/\lambda, \quad (4)$$

$$m = n - ik, \quad (5)$$

where C_{ext} is the extinction cross-section of a single aerosol, R is the aerosol radius and Q_{ext}, Q_{sca}, Q_{abs} are the dimensionless extinction, scattering and absorption efficiencies respectively. The dimensionless size parameter is denoted by x, the wavelength of illuminating radiation by λ and the complex refractive index of the aerosol by m. Figure 1, using $m = 1.51 - 0.0i$, is representative of homogeneous spheres made of ordinary crown glass. The range of aerosol sizes used in this calculation corresponds to the measured range of sizes for the Emerson and Cuming FTF-15 aerosols (henceforth referred to as FTF-15 aerosols). Figure 2, with $m = 1.5 - 0.1i$, depicts the behavior

of a similar glass with an absorbing dye added. Figures 3-5 are included to show the increase in spacing between extinction peaks which result from decreasing the refractive index.

The second stage of development of optical models consisted of the much more difficult task of developing a model for composite or hollow spheres. The original formulation of the solution as given by Güttler (1952), also appearing in Wickramasinghe (1973), was found to be accurate and stable only for aerosols whose product of radius and refractive index fell below a certain value. For aerosols sizes and refractive indices in the range of interest for the problem under consideration, the equations were found to be numerically unstable. The equations were rewritten in a numerically stable but analytically equivalent form and now give satisfactory results for all ranges of input parameters. The model was tested against the published results of Battan et al. (1970), Wickramasinghe (1973) and, in the limit of shell and core materials of the same refractive index, against the results of the homogeneous sphere model.

Figures 6-19 represent a sample of results from the optical model for composite spheres. The modeled aerosol consists of two concentric spheres composed of two different materials. Notation is consistent with that of the earlier model with the addition of m_1 and m_2, which denote the refractive indicies of the core (inner sphere) and shell (outer sphere), respectively. The core radius is denoted by R_0 and the shell's outer radius by R, where $R-R_0$ is the shell thickness in μm. Figures 6-19 show the behavior of a hollow glass sphere aerosol, composed of fused quartz. These results are very different in appearence from those of the solid glass spheres. Qualitatively, this departure can be understood as a combination of two phenomena, a solid sphere of variable refractive index at large aerosol radii and a thin film interference phenomenon at small aerosol radii. The long,

slowly-damped tails and lack of extinction peaks for large aerosol radii can be simulated by a solid glass sphere whose index of refraction decreases with increasing size. Figures 20 and 21 show the results of such calculations, where the indices of refraction were taken to be

$$m = \frac{(1.45)(R-R_0) + 1.00(R_0)}{R} + 0.0i, \qquad (6)$$

with $R-R_0$ = 1.0μm, 2.0μm for Figures 20 and 21 respectively. Equation (6) merely represents a linearly averaged refractive index for a hollow glass sphere. The behavior exhibited in Figures 20 and 21 can easily be understood as an extention of the results presented in Figures 3-5. The resonant minima and maxima in Q_{ext} (Figures 6-19), for small aerosol radii, can be thought of as a thin film interference phenomena. The observed dependence on shell thickness leads to this hypothesis, however the dependence can by no means be completely described by simple thin film interference formula.

II. Emerson and Cuming aerosols, physical measurements

Examination of the physical properties of the FTF-15 aerosols began with a preliminary investigation using the University of Wyoming's Scanning Electron Microscope facility. This investigation was intended to determine whether their size distribution and shell thickness could accurately be measured with such an instrument or whether different methods needed to be explored. A decision was reached that the scanning electron microscope was well suited for accurate determination of size distribution and for approximate determination of shell thickness.

Figure 22 is a photograph taken through the electron microscope, of FTF-15 aerosols mounted on a suitable substate. This photo is one of a series taken expressly for size determination purposes. A magnification of 300 was used on the electron microscope, followed by additional photographic enlargement; a 15μm scale is indicated on the Figure. Mechanical counting and sizing of such photographs lead to the size distribution shown in Figure 23. Shown is the raw data, taken with 1μm resolution in diameter Figures 24 and 25 are the same data smoothed to 2μm and 5μm resolution respectively. The mode of the distribution occurred at 13μm diameter, the mean at 18μm and the spread from 5 to 7μm. The distribution rises sharply from the minimum to the mode diameter then exhibits a slow, exponential-like tail at large sizes.

Figure 26 is an electron microscope photograph of FTF-15 aerosols after they have been crushed with a mortar and pestal. The microscope magnification was 1000, followed by additional photographic enlargement; a 4μm scale is indicated on the Figure. With the aid of this and similar photographs, an upper limit of 1μm could be placed on the aerosols' shell thickness. The aerosol fragments are all fragments of spherical shells. Hence, even if viewed edgewise, their apparent thickness will always exceed the actual shell thick-

ness. Consequently, this technique can only give an upper limit to shell thickness.

A second and more accurate means of determining shell thickness, involving density measurements, was devised. First, a few cm^3 sample of aerosols was suspended in water, in a hypodermic syringe, and the combined volume measured. A hypodermic syringe was needed because unless the aerosol liquid suspension was put under some pressure, the aerosols would float atop the liquid rather than be submerged in it. The volume of the water and the mass of the aerosols were then determined, allowing for calculation of the true average density of the aerosols. Multiple trials yielded .268 g/cm^3 ± 2% for the FTF-15 hollow glass spheres. Knowing the true density of the bulk material of which they are composed, allows for calculation of a mean wall thickness. By this method, the mean wall thickness of the FTF-15 hollow glass spheres is 0.45μm, not at variance with the upper limit of 1μm from microscopic methods.

The final input parameter required for the optical model is that of refractive index. The manufacturer was unable to give us a bulk sample of glass for measurement, as the glass is mixed in the liquid state and then directly formed into aerosols. The manufacturer however, seemed somewhat certain that the glass was similar to boro silicate crown, which has a refractive index of 1.51-0.0i at 1.06μm. Consequently, we used this value in all of our early work. Later, however we received a private communication from Huffman (University of Arizona) stating quite conclusively, based on melting tests and refractive index measurements in the visible, that the FTF-15 aerosols were composed of fused quartz. Consequently, we used the index for fused quartz, 1.45-0.0i at 1.06μm, for the final calculations included in this report.

III. Applications of the Optical Model

Combining the previously measured size distribution, the .45μm shell thickness and the refractive index of 1.45-0.0i, we are now able to calculate volume extinction coefficients for the FTF-15 aerosols. The volume extinction coefficient, β_{ext}, is defined as

$$\beta_{ext} = N \cdot 10^{-3} \cdot \int_0^\infty \pi r^2 \, Q_{ext}(m, 2\pi r/\lambda) C \, n(r) dr, \qquad (7)$$

where β_{ext} is in km^{-1}, N the aerosol number density in cm^{-3}, r the aerosol radius in μm . Attenuation of a collimated light source, such as a laser, can then be calculated simply from Beer's Law,

$$F = F_0 \exp\{-\beta_{ext} \cdot L\} \qquad (8)$$

where F_0 is the flux density (W/cm^2) incident upon the medium, F the flux density exiting the medium and L the length of traverse in the medium. If the optical properties of the medium are not homogeneous, then the simple $\beta_{ext} \cdot L$ product is replaced by an integration of β_{ext} over the path traversed.

Table 1 gives the volume extinction coefficient for the FTF-15 aerosols, for various values of suspended number densities N.

Table 1

$N(cm^{-3})$	$\beta_{ext}(km^{-1})$	$N(cm^{-3})$	$\beta_{ext}(km^{-1})$
.01	1.22×10^{-2}	5.00	6.09
.05	6.09×10^{-2}	10.00	1.22×10^{1}
.10	1.22×10^{-1}	50.00	6.09×10^{1}
.50	6.09×10^{-1}	100.00	1.22×10^{2}
1.00	1.22		

β_{ext} of course just scales as a multiple of N, since N is just a constant which multiplies the integral in Eg. (7). To obtain a feeling for aerosol number densities, one should note that naturally occurring stratospheric aerosols have typical number densities of $1.0cm^{-3}$ and naturally occurring tropospheric aerosols have number densities of $\geq 10^2 cm^{-3}$. However, these naturally occurring aerosols have volume extinction coefficients of only $10^{-3} - 10^{-4}$ km^{-1} and $10^{-1} - 10^{-2}$ km^{-1} respectively. The descrepancy in

the ratio of β_{ext}/N for naturally occurring versus FTF-15 aerosols stems from the fact that the FTF-15 aerosols are orders of magnitude larger in size, the factor r^2 being very prominent in Eg. (7).

Certain practical questions regarding the implementation of the FTF-15 can easily be answered from the results of Table 1. For instance, if it were desired to produce a β_{ext} of ~ $1.0km^{-1}$ over a volume of $1km^3$, a total of 10^{15} aerosols would have to be approximately evenly dispersed over the 1 km^3 volume.

The second primary application of the optical model was to investigate the question, whether other types of aerosols might be a better or somehow optional choice for producing extinction of 1.06μm radiation. To this end, the optical model was used to calculate extinction coefficients for aerosols of differing size distributions, shell thickness and refractive indices.

Regarding the question of varying size distributions, one could make a detailed, but unrealistic study of various monodisperse aerosols. However, truly monodisperse aerosols are difficult or impossible to produce by high volume manufacturing processes. Hence, I choose to take the measured FTF-15 aerosol size distribution and shift it to larger or smaller sizes by multiplying each size bin by some constant S. This procedure produced a distribution which maintained the original, realistic shape, but contained larger or smaller mean diameters. Specifically, if the original distribution had a mean diameter of 18μm, a spread of 5-51μm and the constant S were given a value of 0.1, then the new distribution would have a mean diameter of 1.8μm and a spread of 0.5-5.1μm. Table 2 presents the results of these calculations, where N = $1cm^{-3}$ was used.

Table 2

S	$\beta_{ext}(km^{-1})$	S	$\beta_{ext}(km^{-1})$
.01	3.35×10^{-6}	1.00	1.22
.03	5.55×10^{-4}	3.00	1.13×10^{1}
.10	1.48×10^{-2}	10.00	1.27×10^{2}
.30	1.09×10^{-1}		

The results are as to be expected, larger aerosols yield substantially greater extinction, for a fixed number density. Furthermore,for large sizes such that most of the aerosols are to the right of the first extinction peak (i.e., see Figures 1-21), β_{ext} is approximately proportional to the mean radius squared which is directly proportional to S^2. However, larger aerosols weigh more and constitute a larger volume of agent to deliver to the designated area. Hence, if the capacity of the delivery system is included, there must be some tradeoffs, to consider.

Let us define a quantity ρ,

$$\rho = N \cdot 10^{-12} \int_0^\infty \frac{4\pi}{3} [r^3 - (r - .45\mu m)^3] \cdot \rho_g \cdot cn(r)dr, \qquad (9)$$

where ρ is the density (g/cm^3) of the aerosol in its suspended state, ρ_g the density of fused quartz, and $N = 1cm^{-3}$. Hence for a given volume into which the aerosol is to be dispersed, ρ is proportional to the mass of aerosol which the delivery system must be capable of handling. Table 3 presents the ratio of β_{ext}/ρ versus S.

Table 3

S	$\beta_{ext}(km^{-1})/\rho(g/cm^3)$	S	$\beta_{ext}(km^{-1})/\rho(g/cm^3)$
.01	2.59×10^8	1.00	9.24×10^8
.03	1.60×10^9	3.00	9.29×10^8
.10	1.63×10^9	10.00	9.32×10^8
.30	1.01×10^9		

The units and absolute magnitudes here are not of great importance, but the relative magnitudes are. These calculations show that an S of around .10 would yield the maximum optical extinction for a given mass of aerosol delivered to the designated area. An S of .10 corresponds to a size distribution with a mean diameter of 1.8μm and a spread of .5 to 5.1μm. It should be noted that the small aerosols produced by S values of less than unity have been assumed to be solid, rather than hollow, when their radius decreased to less than .45μm. This assumption is con-

sistent with a constant shell thickness under conditions of a variable size distribution.

The results of Table 3 can be easily understood if one makes use of the fact that ρ is approximately proportional to r^2 for large S values, and to r^3 for small S values. Also β_{ext} is approximately proportional to r^2 for large S values and proportional to r^6 for small S values. This explains the observed behavior that β_{ext}/ρ is nearly constant for $.3 \leq S \leq 10.0$, and drops off to its smallest values at S = .01.

A second means of including delivery system capacity in tradeoff decisions, is to calculate the packed volume of the aerosols which need to be delivered to the designated area. Since the packed aerosols are of such small density ($.16 g/cm^3$), the volume rather than mass might be a more important quantity to consider.

To this end, we define a quantity V,

$$V = \frac{.268}{.16} \cdot N \cdot 10^{-12} \cdot \int_0^\infty \frac{4}{3} \pi r^3 \cdot C\, n(r) dr, \qquad (10)$$

which is dimensionless and equal to the packed volume of aerosol per unit of suspended volume. The number density N remains 1 cm^{-3} and the ratio .268/.16 represents the ratio of true (liquid immersion) to packed density of the FTF-15 aerosols. Hence, for a fixed volume over which the aerosol is to be dispersed, the ratio of β_{ext}/V gives the optical extinction per unit volume of delivery system.

Table 4

S	$\beta_{ext}(km^{-1})/V$	S	$\beta_{ext}(km^{-1})/V$
.01	2.71×10^8	1.00	9.87×10^7
.03	1.67×10^9	3.00	3.40×10^7
.10	1.20×10^9	10.00	1.03×10^7
.30	3.27×10^8		

These results show a greater variance with S than for Table 3, resulting from the fact that V is directly proportional to r^3 for all values of S. The results show that S values of .03 to .10, a substantially

smaller aerosol than the FTF-15, would be the optional choice if the volume which could be carried by the delivery system was a limiting factor.

A second major consideration in searching for an optional aerosol for the extinction of 1.06μm radiation is that of varying the shell thickness of the hollow glass spheres. Table 5 presents the results of this study, where N was again fixed at $1.0cm^{-3}$.

Table 5

R-Ro(μm)	$\beta_{ext}(km^{-1})$	R-Ro(μm)	$\beta_{ext}(km^{-1})$
1.25	.771	.53	.992
1.06	.378	.50	1.08
1.00	.464	.45	1.22
.79	.650	.40	1.19
.75	.791	.35	1.06
.60	.957	.26	.834
.55	.959	.25	.802

These results show that our measured mean shell thickness of .45μm, for the FTF-15 aerosols,is approximately tuned to the 1.06μm wavelength and maximizes extinction. The results presented in Table 5 follow directly from the Q_{ext} calculations shown in Figures 6-19. It should be pointed out that variations in shell thickness produce a variation of at most a factor of three in β_{ext}, whereas variations in size distribution produced orders of magnitude changes in extinction.

A third major consideration in optimizing aerosol extinction is that of producing FTF-15 like aerosols composed of a different substance. To that end, Table 6 shows the effect of varying the refractive index.

Table 6

m_1	m_2	$\beta_{ext}(km^{-1})$
1.00-0.0i	1.33-0.0i	1.07
1.00-0.0i	1.40-0.0i	1.20
1.00-0.0i	1.45-0.0i	1.22
1.00-0.0i	1.50-0.0i	1.15
1.00-0.0i	1.55-0.0i	1.02
1.00-0.0i	1.60-0.0i	.89
1.00-0.0i	1.65-0.0i	.83
1.00-0.0i	1.70-0.0i	.78
1.00-0.0i	1.33-0.1i	.90

Table 6 continued

m_1	m_2	$\beta_{ext}(km^{-1})$
1.00-0.0i	1.70-0.1i	.77
1.33-0.0i	1.45-0.0i	.73
1.45-0.0i	1.45-0.0i	.74
1.70-0.0i	1.45-0.0i	.74
1.33-0.1i	1.45-0.0i	.73

Number density again was fixed at $1.0cm^{-3}$. A refractive index of 1.33-0.0i corresponds to water, and m = 1.70-0.0i corresponds to very dense flint glasses. Imaginary indices greater than zero correspond to adding absorbing dyes to the basic substance. Surprisingly, the refractive index of fused quartz seems approximately tuned to the 1.06μm radiation just as was the .45μm shell thickness. However, varying the refractive index of both core and mantle has an even smaller effect on changing the extinction than did varying the shell thickness. Hence aerosol composition is the least important of the variables studied.

In concluding the study to optimize aerosol extinction at 1.06μm, we must remark that we have by no means conducted an exhaustive study. Clearly there are endless combinations of variables which were not tried. However, we did allow each of the input parameters to the optical model to vary independently of each other and studied the response regarding extinction. We conclude that size distribution variations have the largest impact on extinction, with shell thickness and refractive index placing a distant second and third respectively. For a given number density, extinction increases proportional to the average size of the aerosol. However, if one is concerned with either the weight or volume capacity of the delivery system, then aerosol distributions with mean diameters of 0.5-1.8μm (10-30 times smaller than the FTF-15) are the optimum choice. The optimum size is much more sharply defined for volume considerations than for weight considerations.

ACKNOWLEDGEMENTS

The author wishes to thank Catherine E. Ryan for her software development and laboratory measurements.

REFERENCES

Battan, L. J., S. R. Browning, and B. M. Herman, 1970. Tables of the Radar Cross Sections of Dry and Wet Ice Spheres, Technical Report No. 21, University of Arizona.

Deirmendjian, D., 1969. Electromagnetic Scattering on Polydispersions, American Elsevier Publishing Co., New York, pp. 290.

Guttler, A. 1952. Die Miesche Theorie der Beugung durch Dielektrische Kugeln mit Absorbierendem Kern und ihre Bedeutung fürProbleme der Interstellaren Materie und des Atmosphärischen Aerosols. Ann der Physik, 6 Fralge, Bd. 11: 65-98.

Kuriyan, J. G., D. H. Phillips, and M. T. Chahive, 1974. Multi-Spectral Extinction Measurements to Deduce the Complex Refractive Index and the Size Distribution of Aerosol Particles, J. Atmos. Sci., 31, 2233-2236.

Mie, G. 1908. Beiträge zur Optik trüber Medien, speziell kolloidaler Metallösungen (Contribution to the optics of suspended media, specifically collidal metal suspensions). Ann. Phys., 25: 377-445.

Wickramasinghe, N. C., 1973. Light Scattering Functions for Small Particles, Adam Hilger, London, pp. 506.

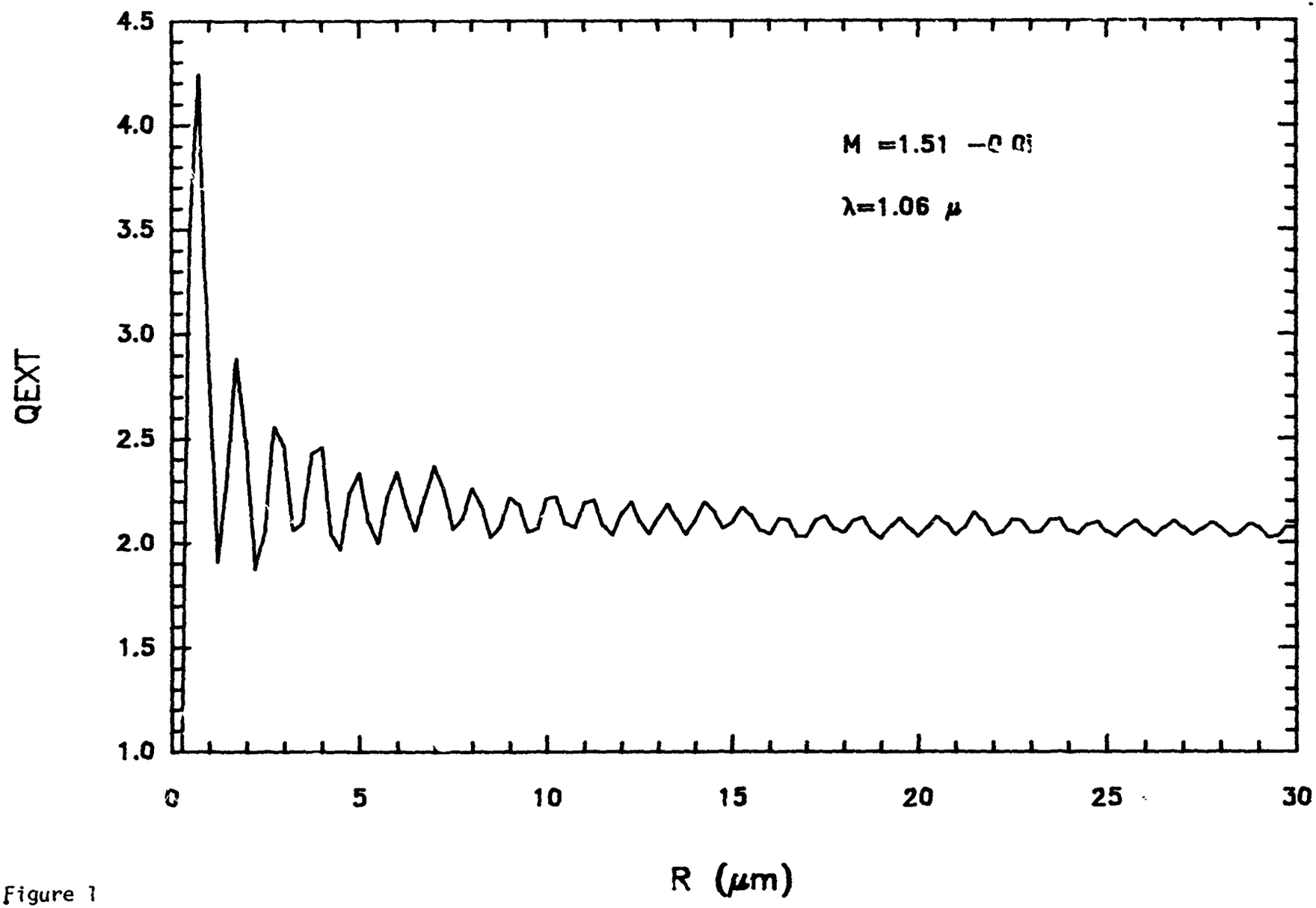

Figure 1

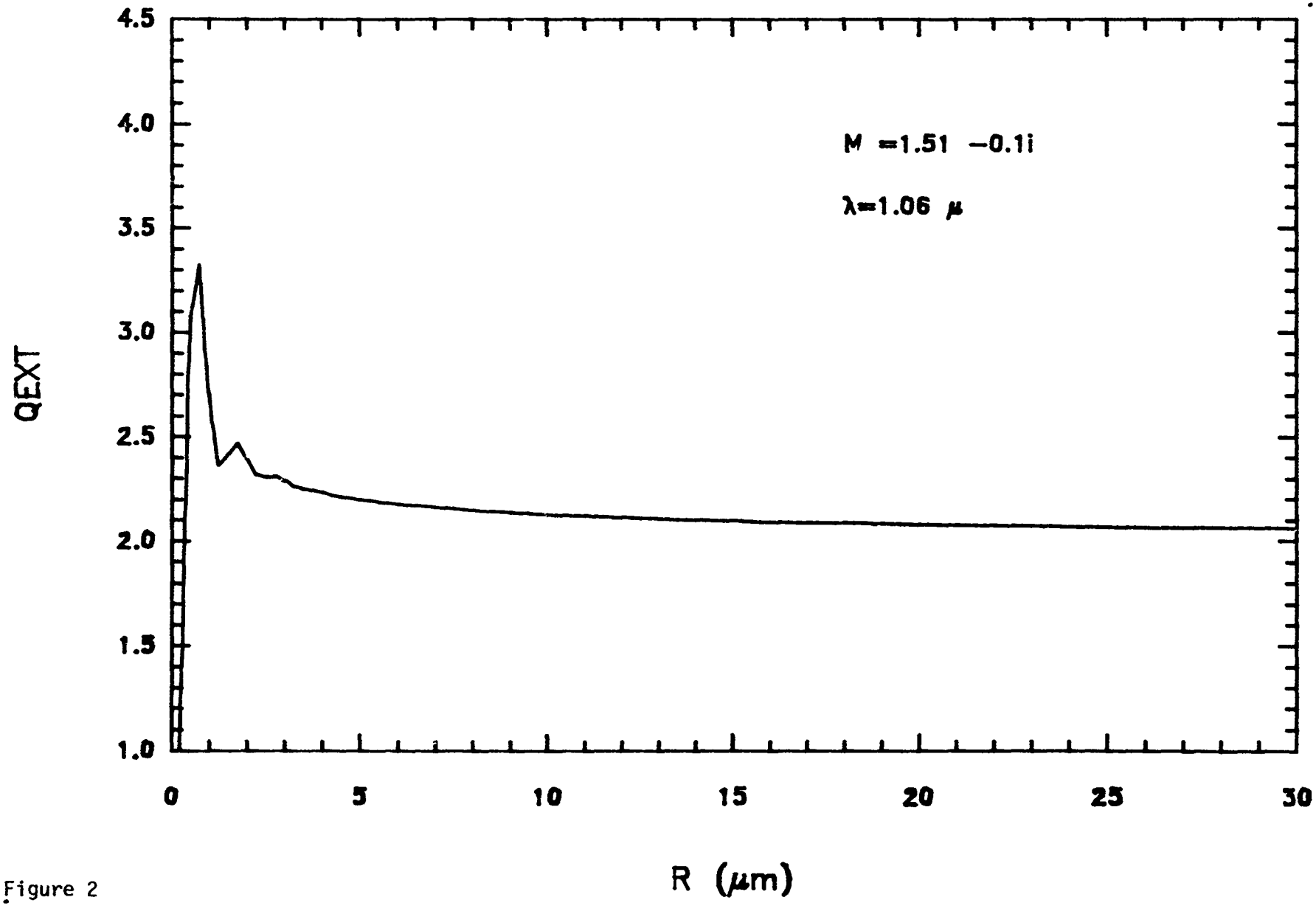

Figure 2

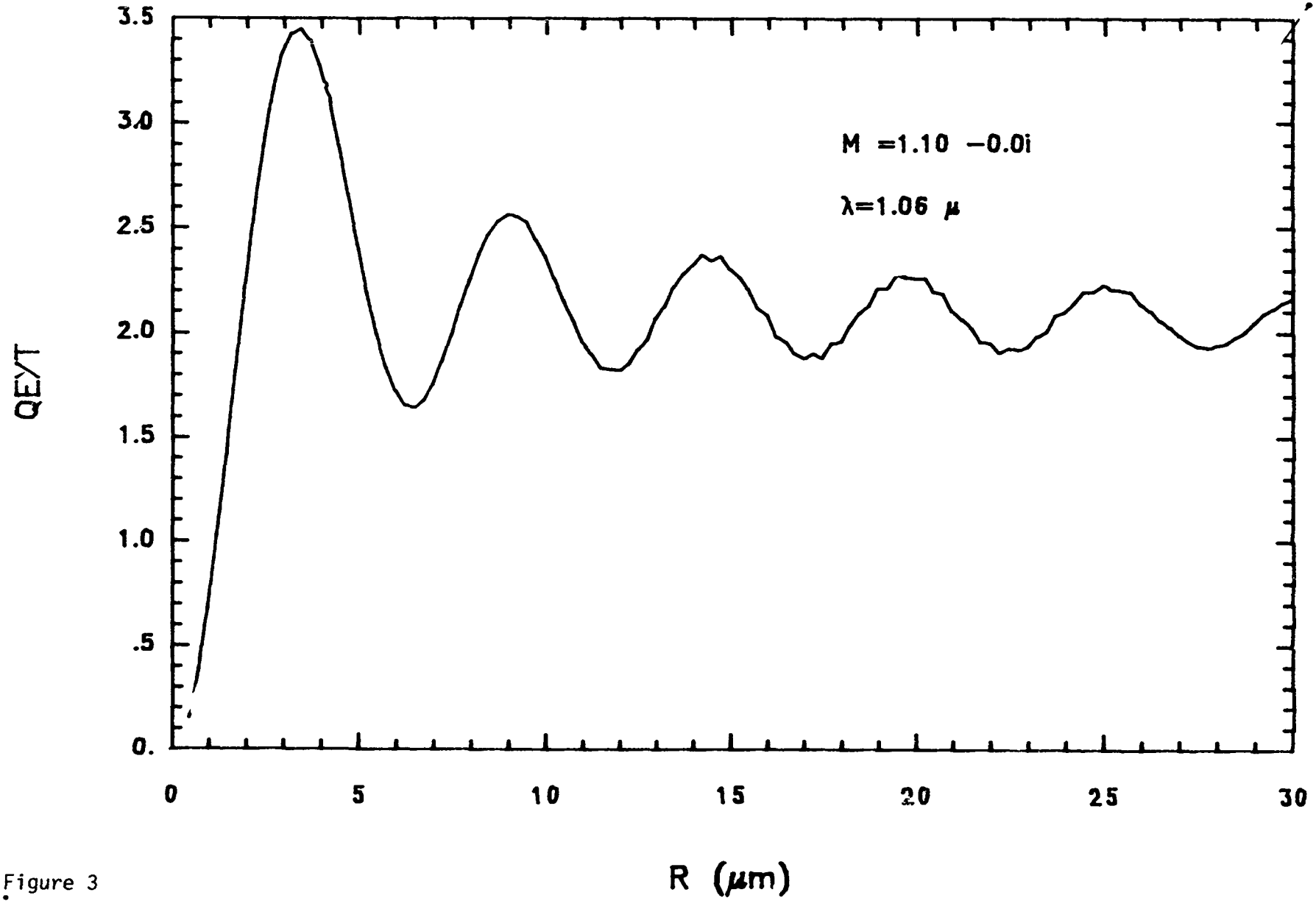

Figure 3

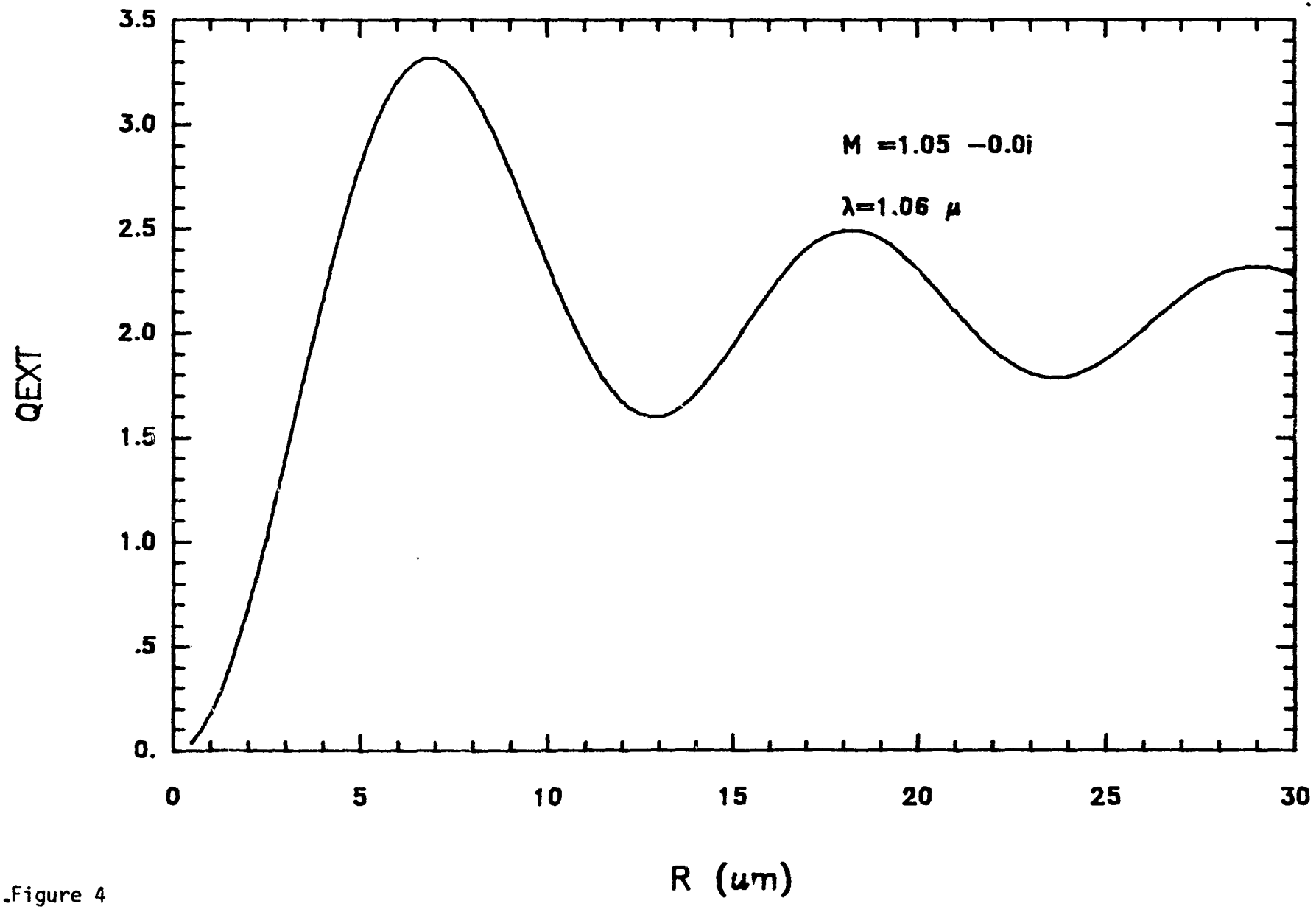

.Figure 4

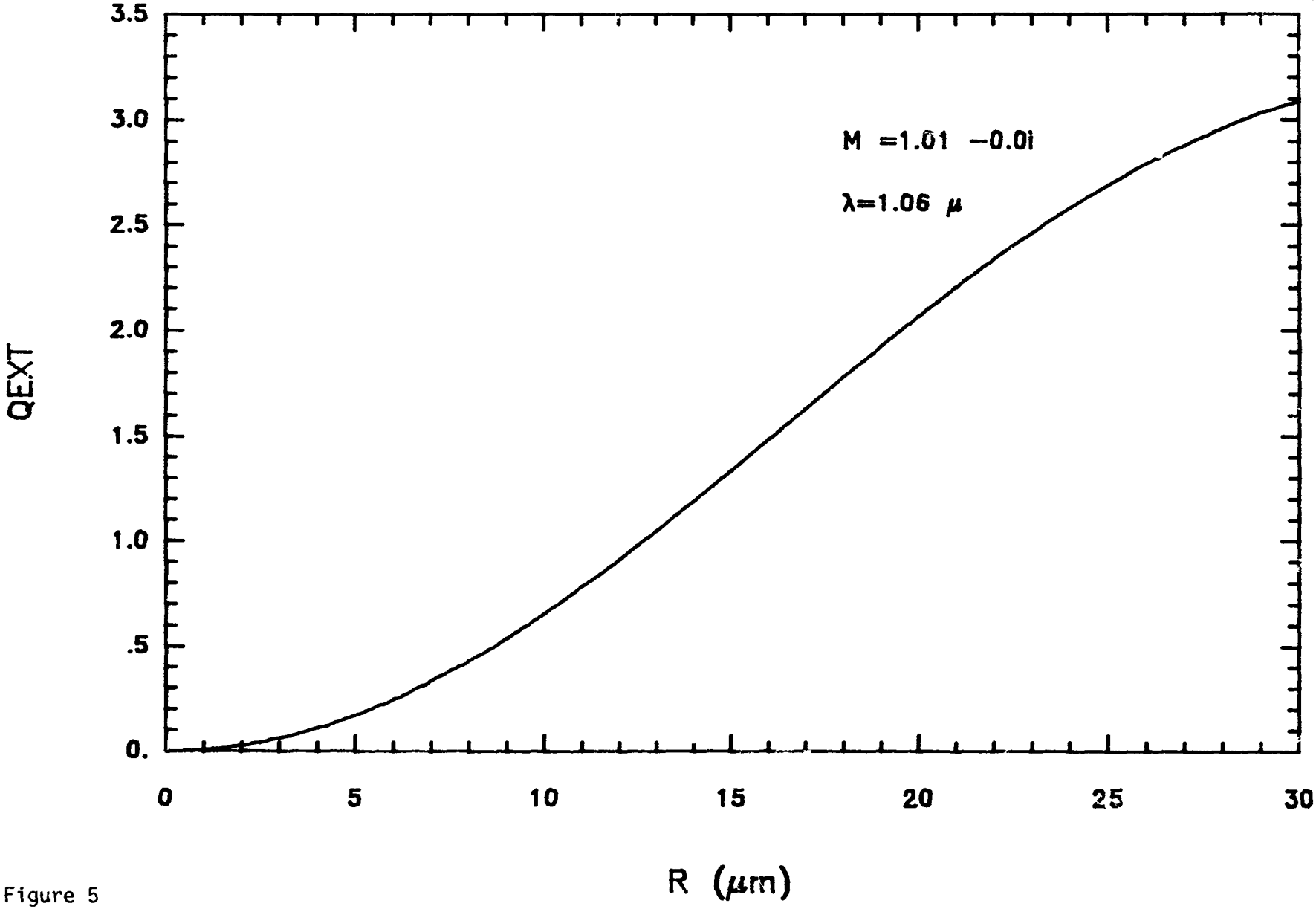

Figure 5

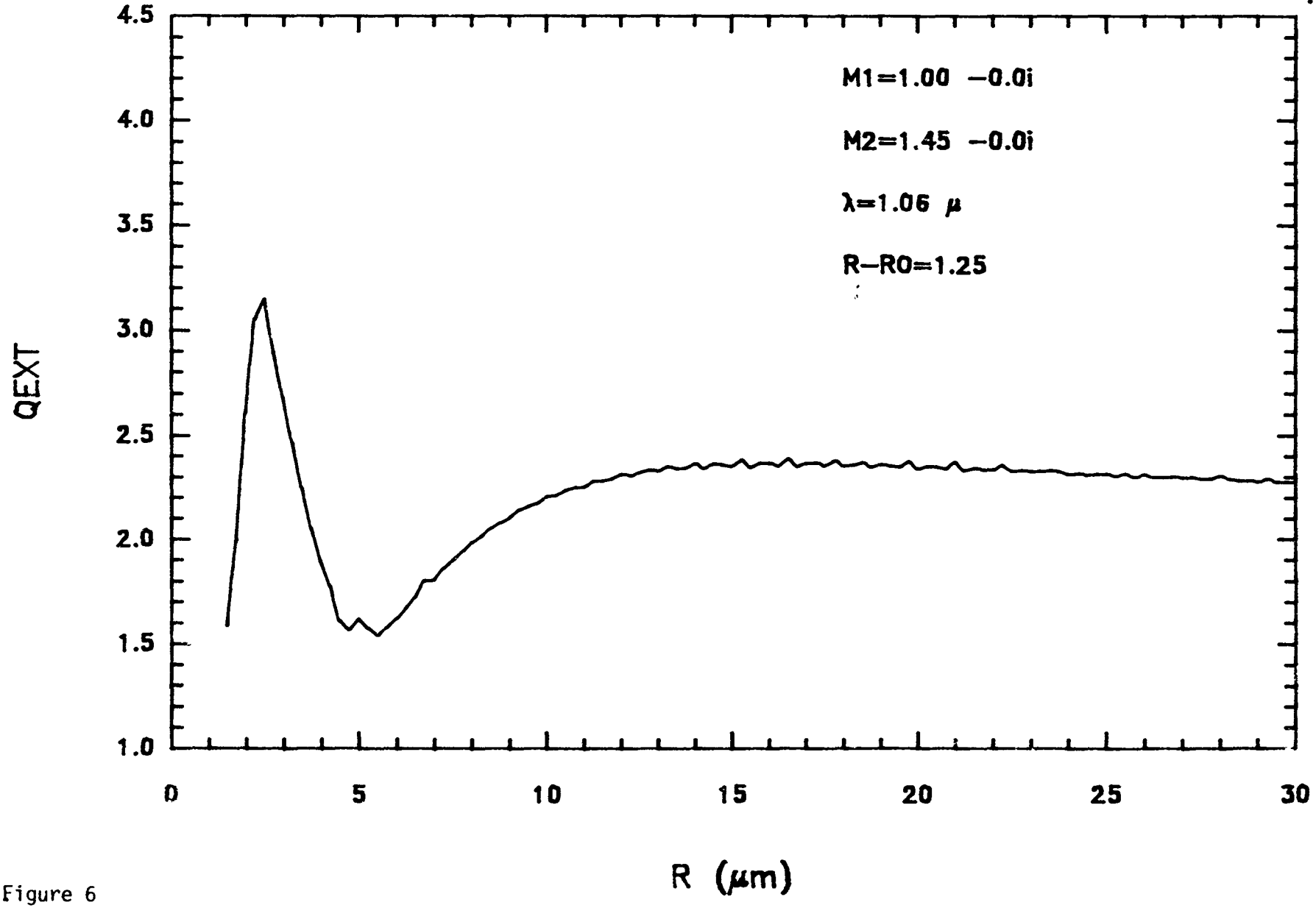
M1=1.00 −0.0i
M2=1.45 −0.0i
λ=1.06 μ
R−RO=1.25
QEXT
4.5
4.0
3.5
3.0
2.5
2.0
1.5
1.0
0
5
10
15
20
25
30
R (μm)

Figure 6

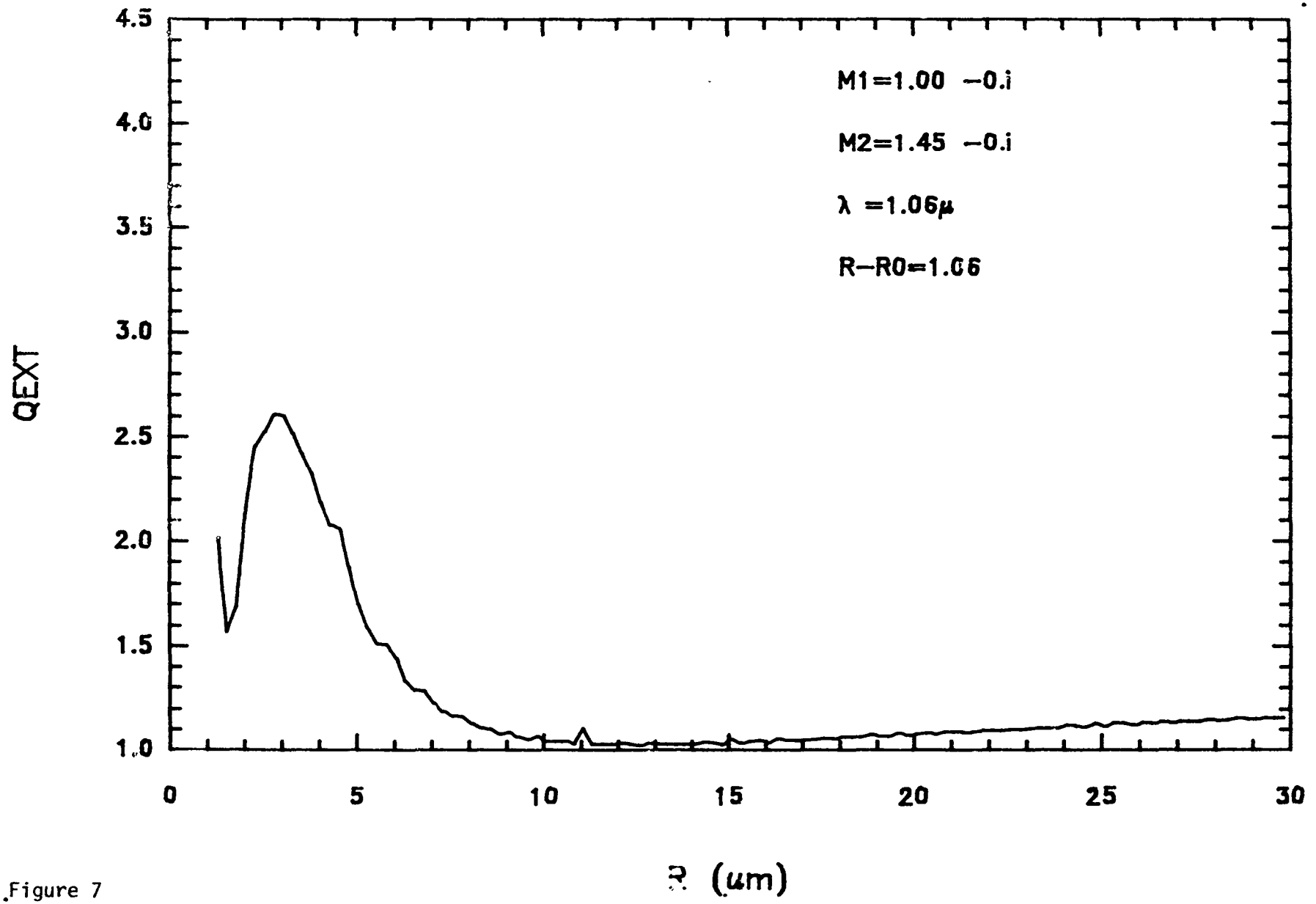
M1=1.00 −0.i
M2=1.45 −0.i
λ =1.06μ
R−R0=1.06
QEXT
4.5
4.0
3.5
3.0
2.5
2.0
1.5
1.0
0
5
10
15
20
25
30
R (μm)

Figure 7

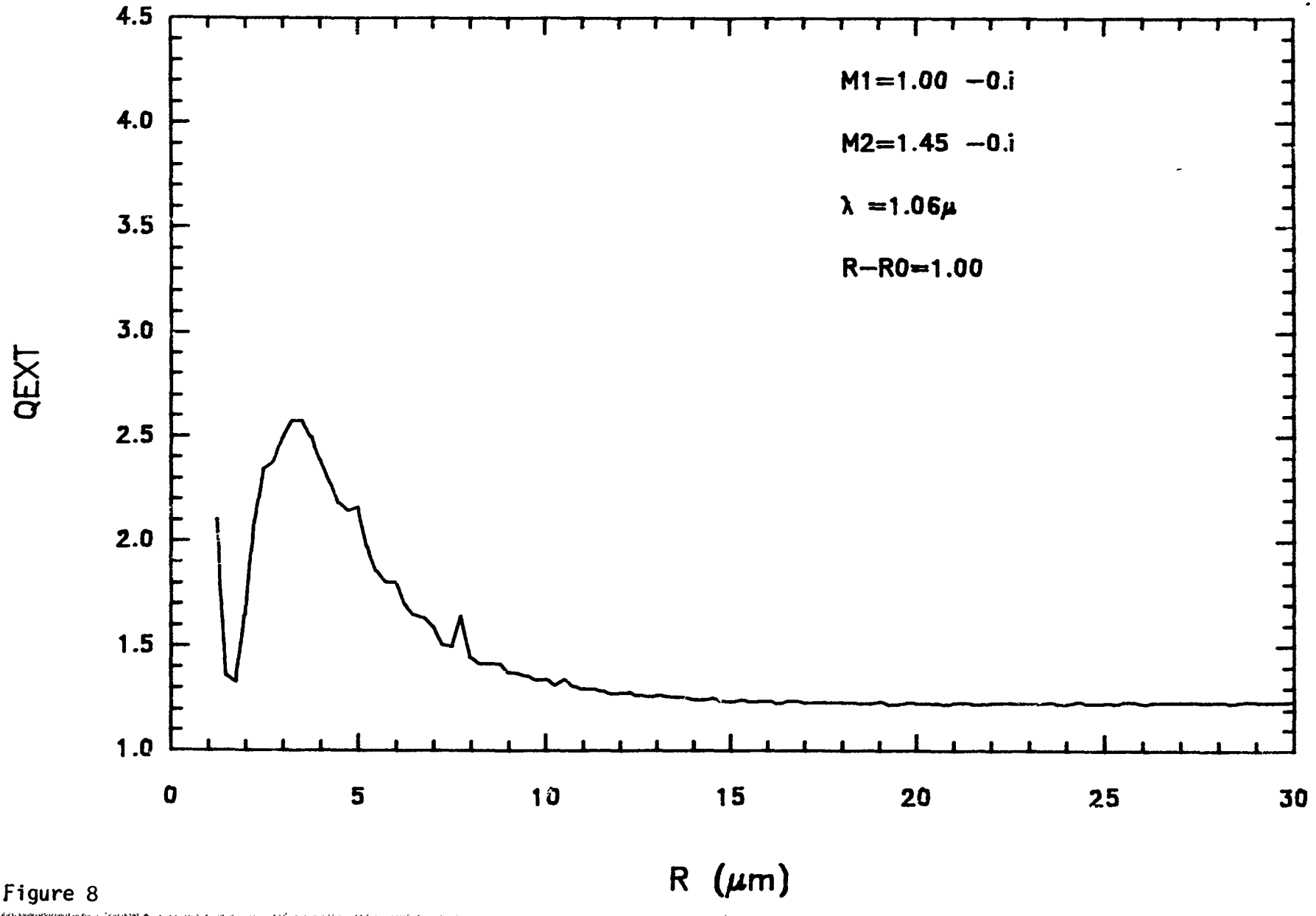
M1=1.00 −0.i
M2=1.45 −0.i
λ =1.06μ
R−R0=1.00
QEXT
4.5
4.0
3.5
3.0
2.5
2.0
1.5
1.0
0
5
10
15
20
25
30
R (μm)

Figure 8

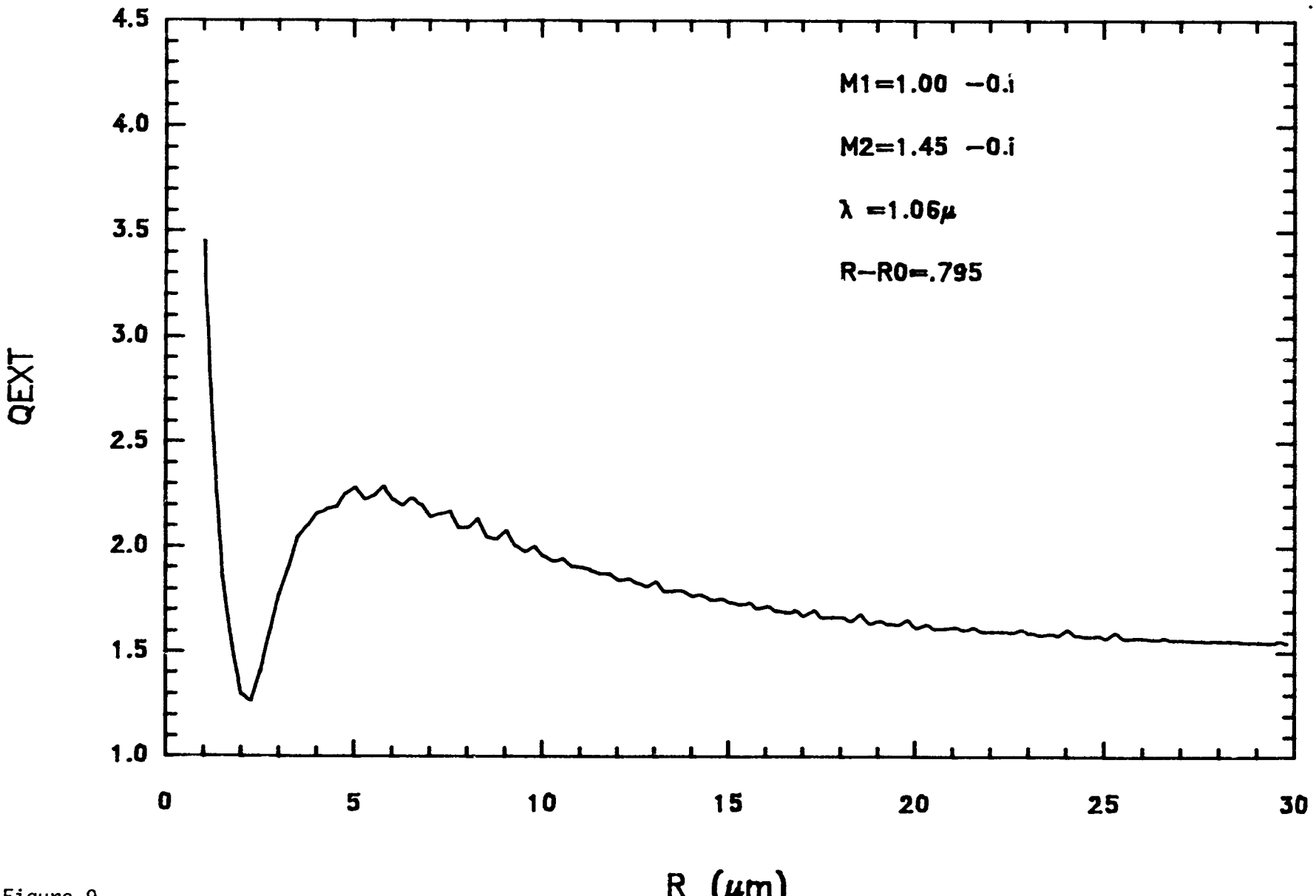
M1=1.00 -0.i
M2=1.45 -0.i
λ =1.06μ
R-R0=.795
QEXT
4.5
4.0
3.5
3.0
2.5
2.0
1.5
1.0
0
5
10
15
20
25
30
R (μm)

Figure 9

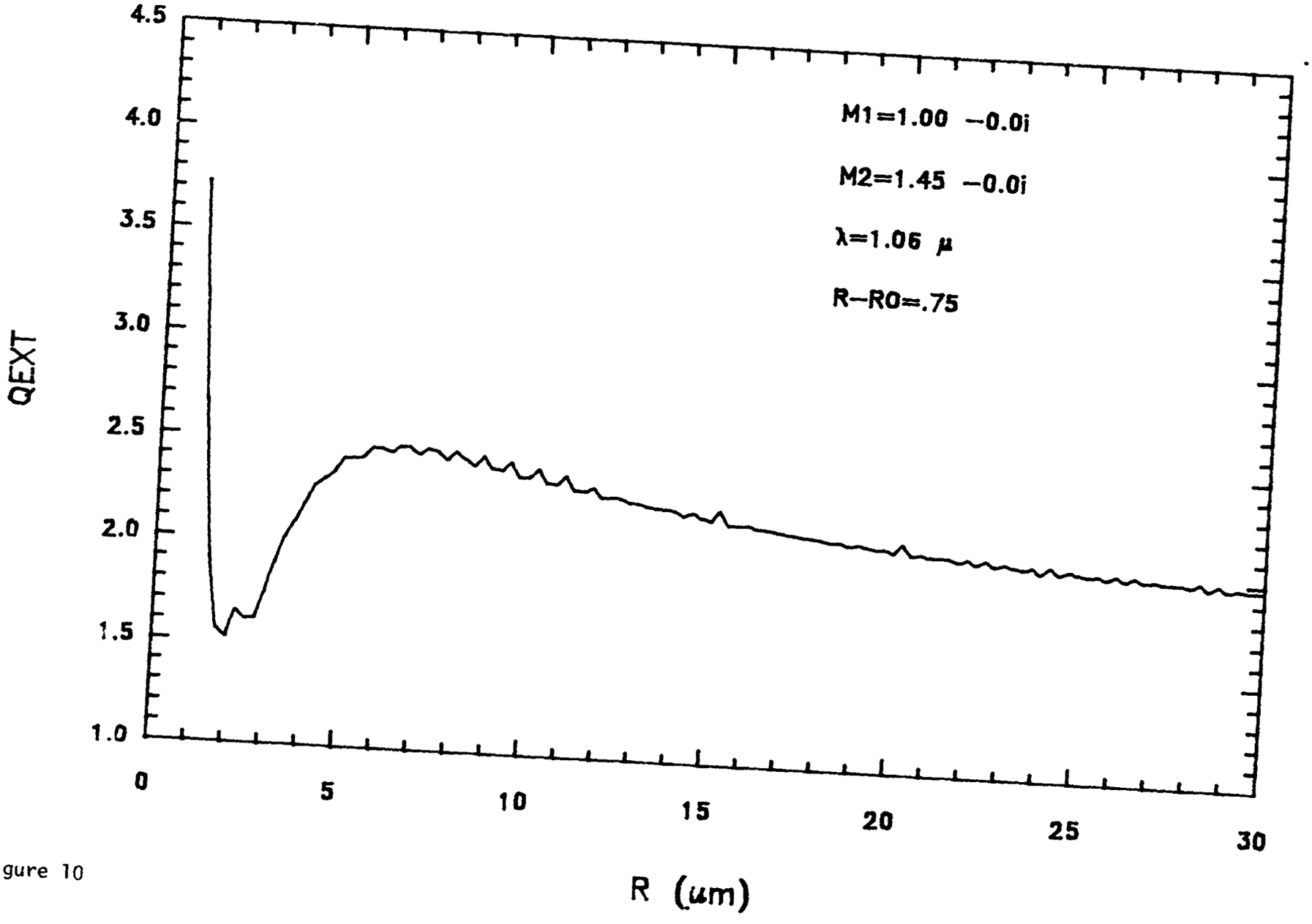
4.5
4.0
3.5
3.0
2.5
2.0
1.5
1.0
QEXT
M1=1.00 −0.0i
M2=1.45 −0.0i
λ=1.06 μ
R−RO=.75
0
5
10
15
20
25
30
R (μm)

Figure 10

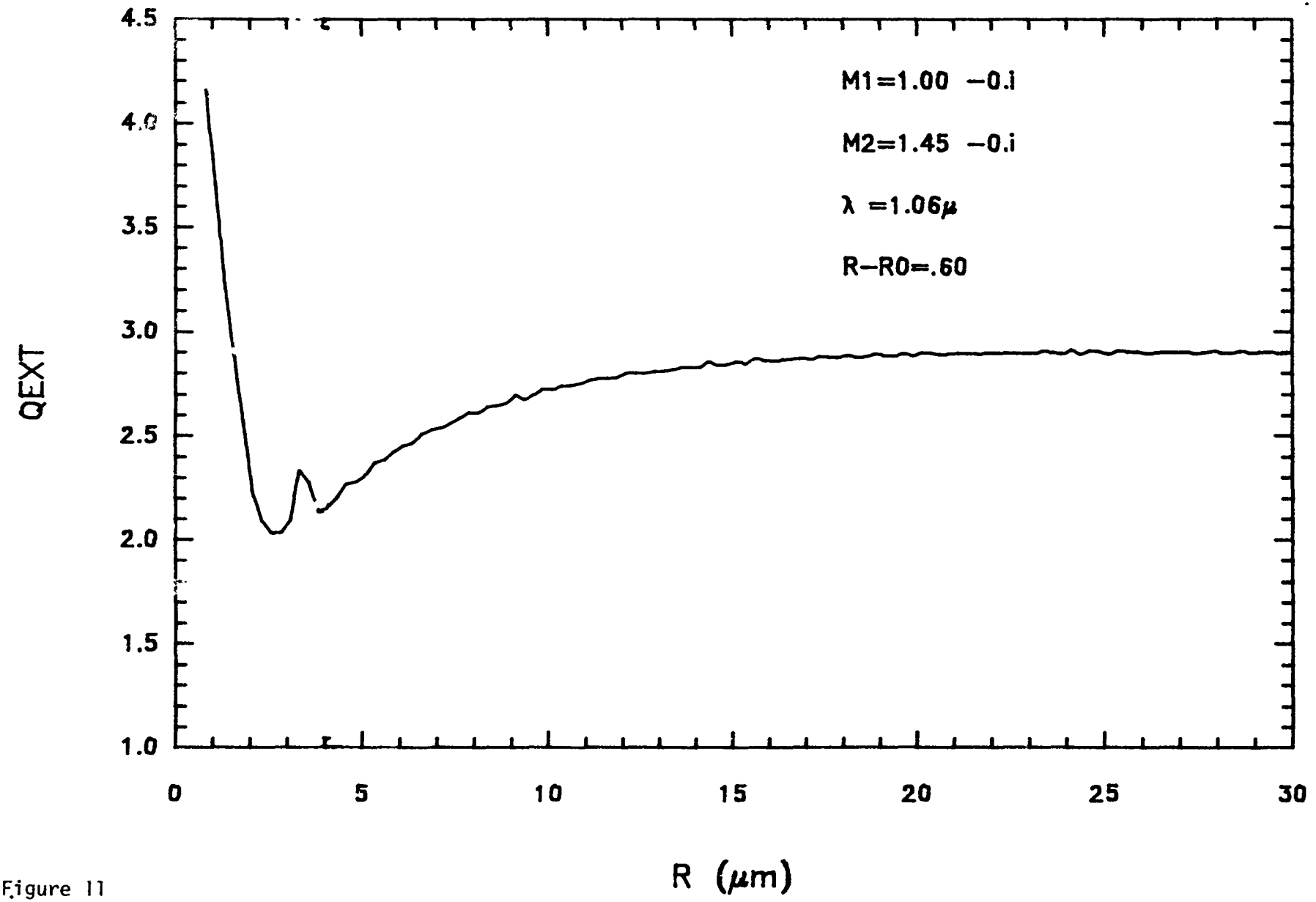
M1=1.00 −0.i
M2=1.45 −0.i
λ =1.06μ
R−R0=.60
QEXT
4.5
4.0
3.5
3.0
2.5
2.0
1.5
1.0
0
5
10
15
20
25
30
R (μm)

Figure 11

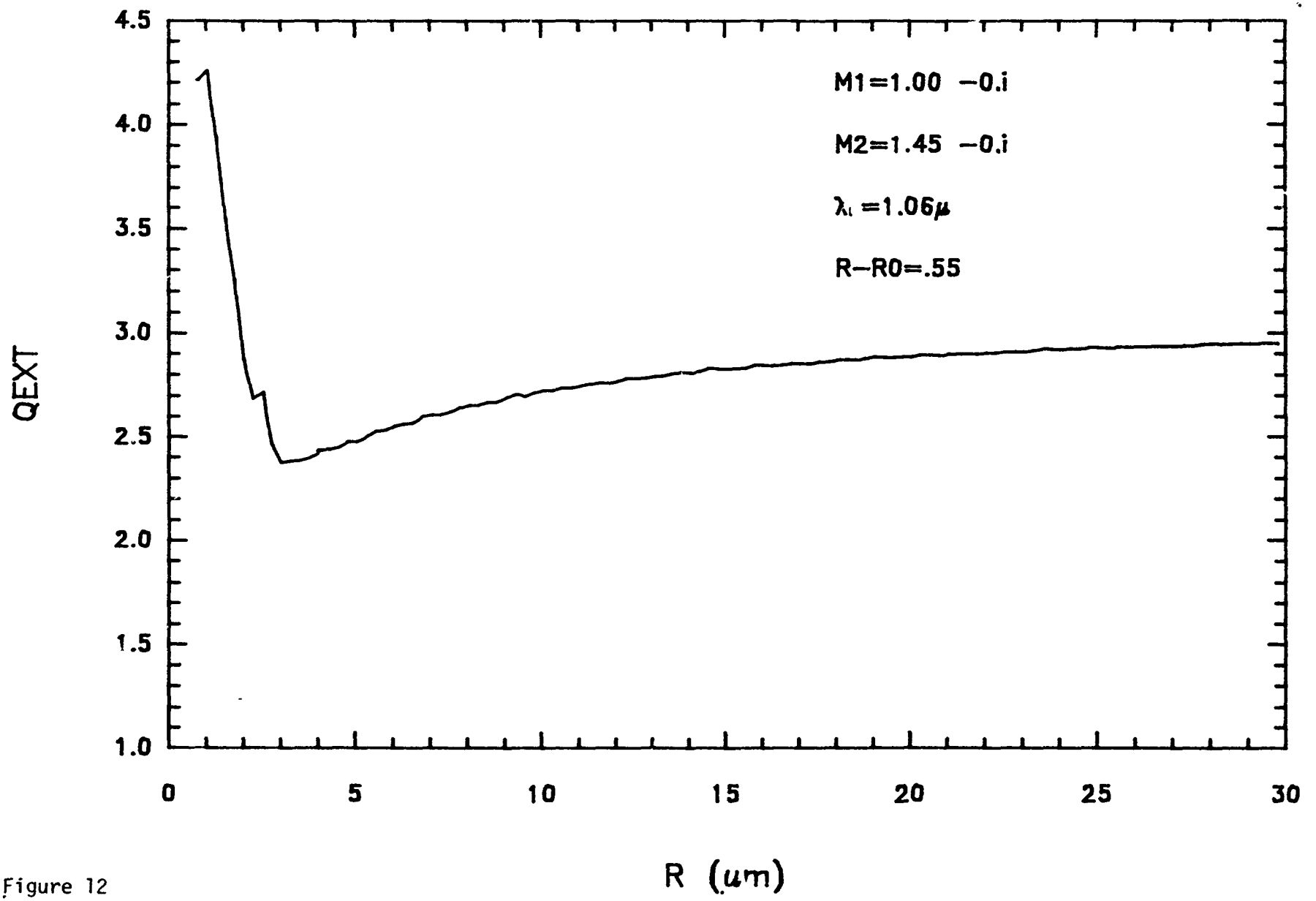
4.5
4.0
3.5
3.0
2.5
2.0
1.5
1.0
QEXT
M1=1.00 −0.i
M2=1.45 −0.i
λ =1.06μ
R−R0=.55
0
5
10
15
20
25
30
R (μm)

Figure 12

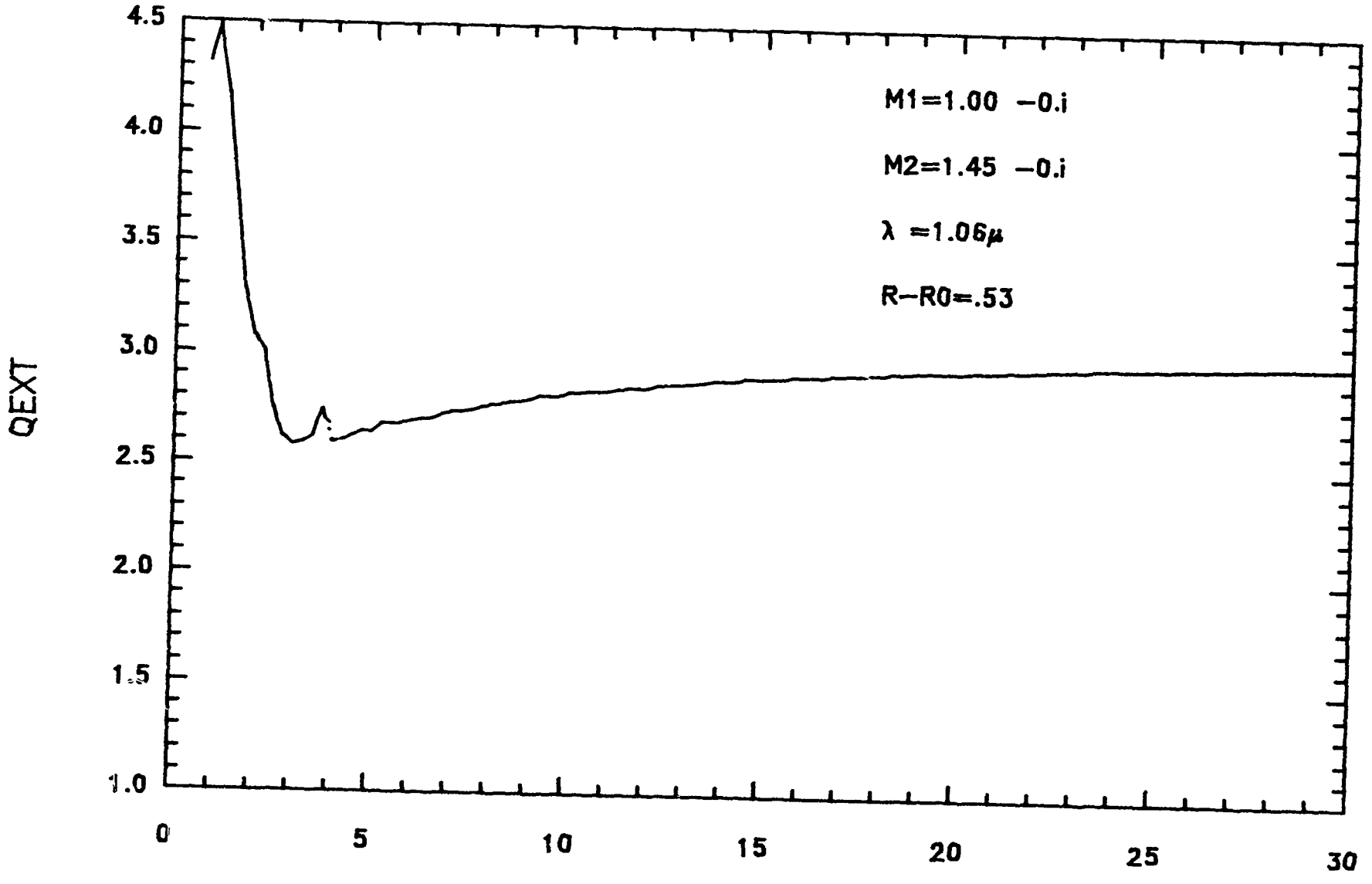
4.5
4.0
3.5
3.0
2.5
2.0
1.5
1.0
QEXT
M1=1.00 −0.i
M2=1.45 −0.i
λ =1.06μ
R−R0=.53
0
5
10
15
20
25
30
R (μm)

Figure 13

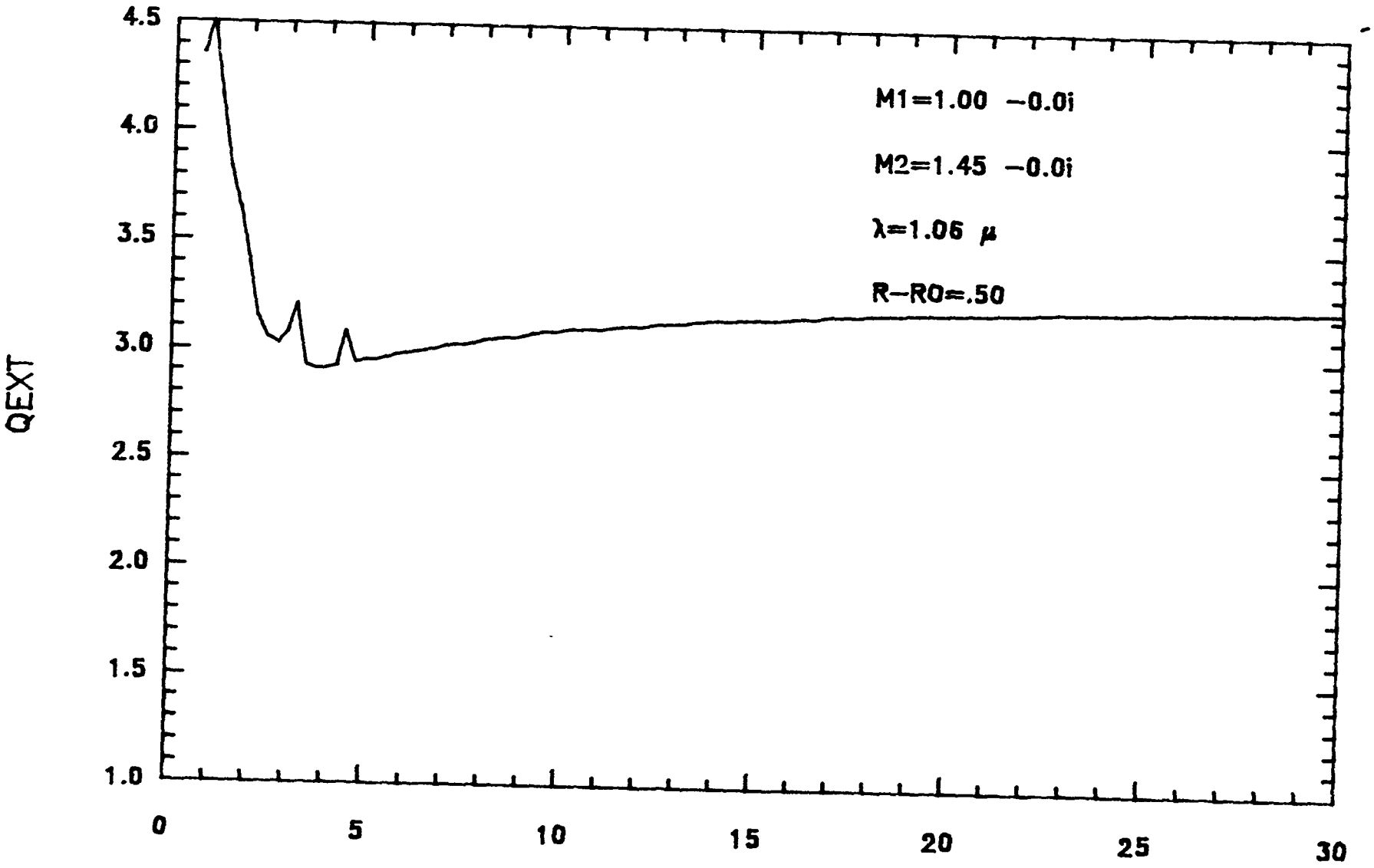
4.5
4.0
3.5
3.0
2.5
2.0
1.5
1.0
QEXT
M1=1.00 -0.0i
M2=1.45 -0.0i
λ=1.06 μ
R-RO=.50
0
5
10
15
20
25
30
R (μm)

Figure 14

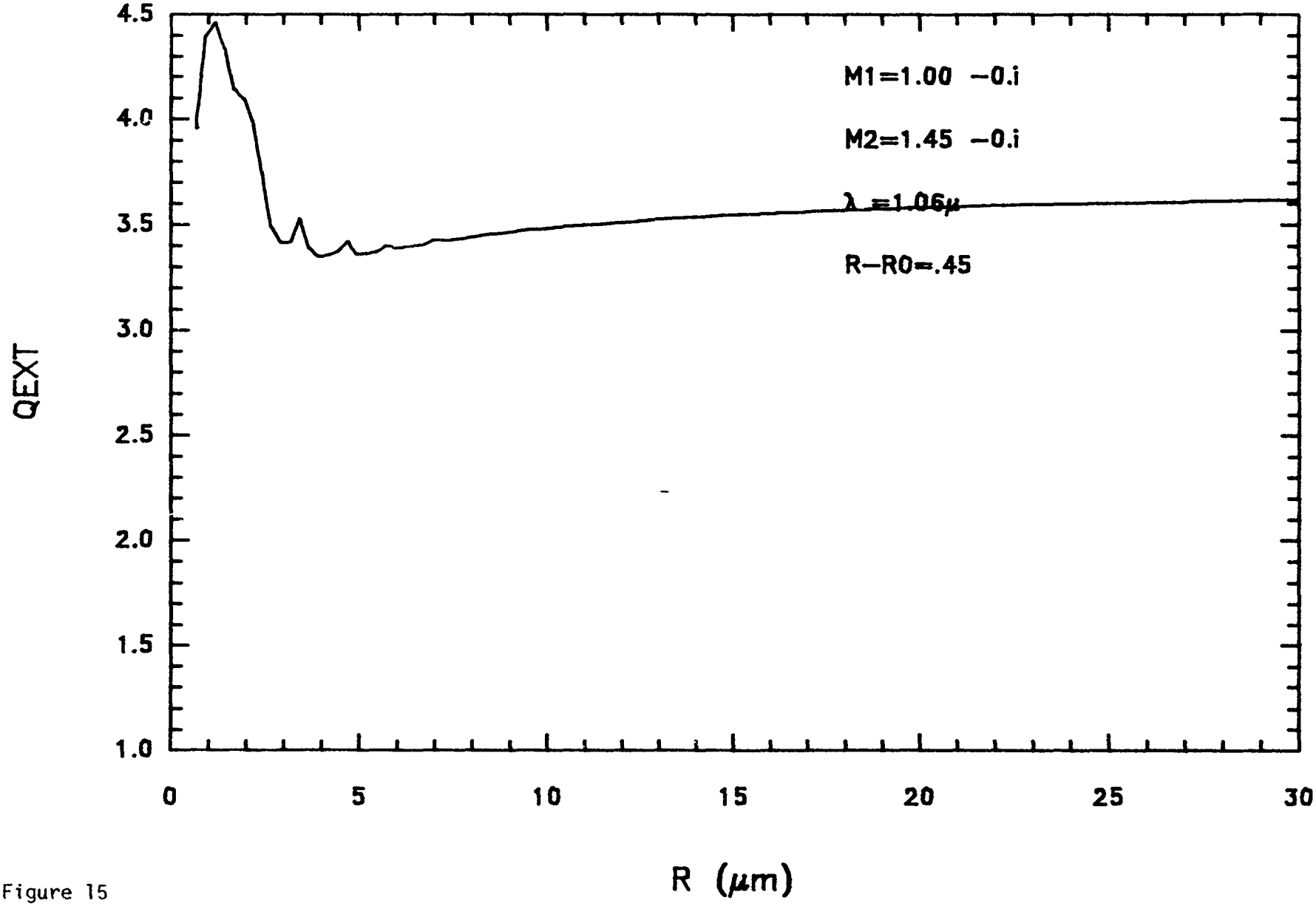
4.5
4.0
3.5
3.0
2.5
2.0
1.5
1.0
QEXT
M1=1.00 −0.i
M2=1.45 −0.i
λ =1.06μ
R−R0=.45
0
5
10
15
20
25
30
R (μm)

Figure 15

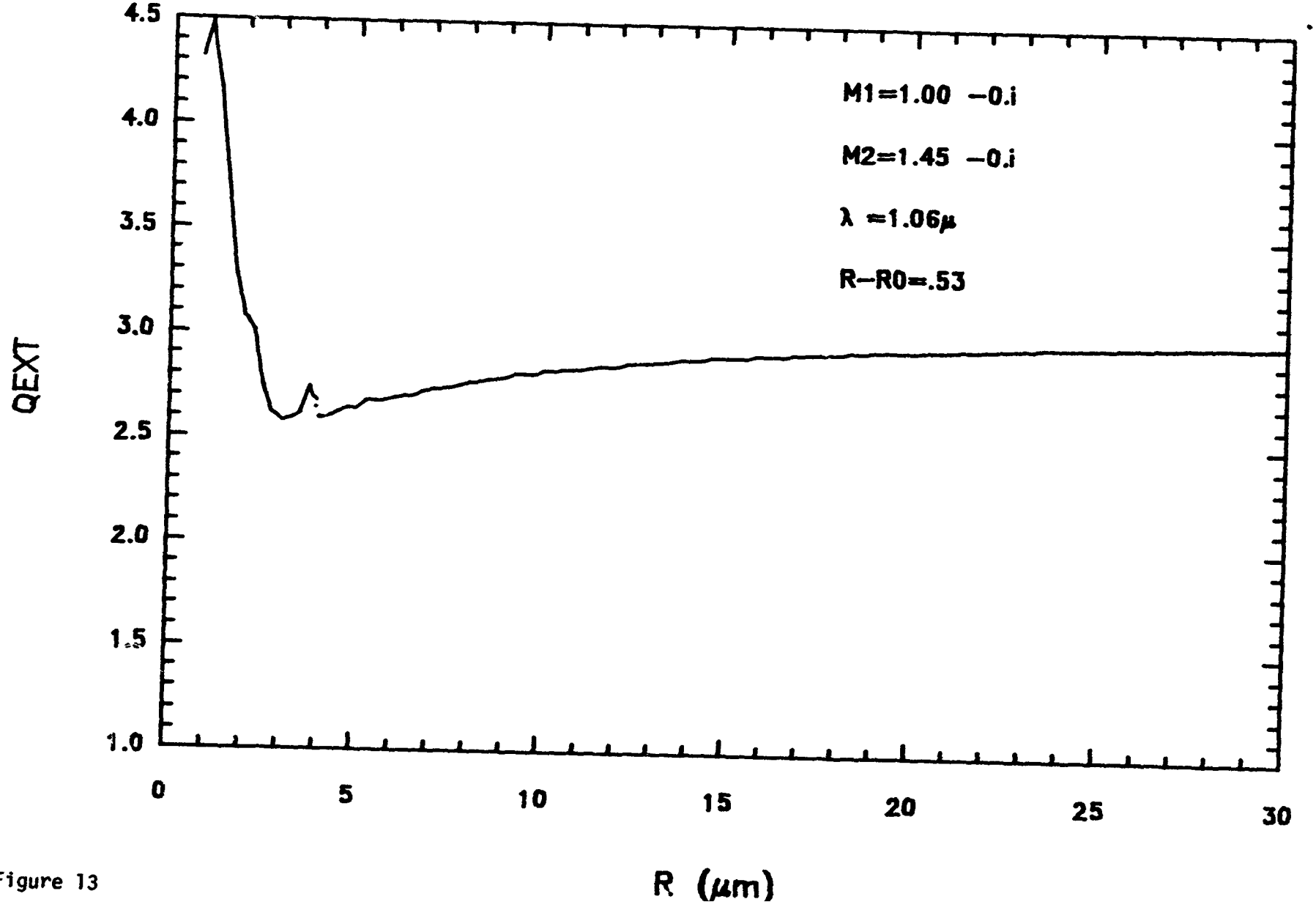
4.5
4.0
3.5
3.0
2.5
2.0
1.5
1.0
QEXT
M1=1.00 -0.i
M2=1.45 -0.i
λ =1.06μ
R-R0=.53
0
5
10
15
20
25
30
R (μm)

Figure 13

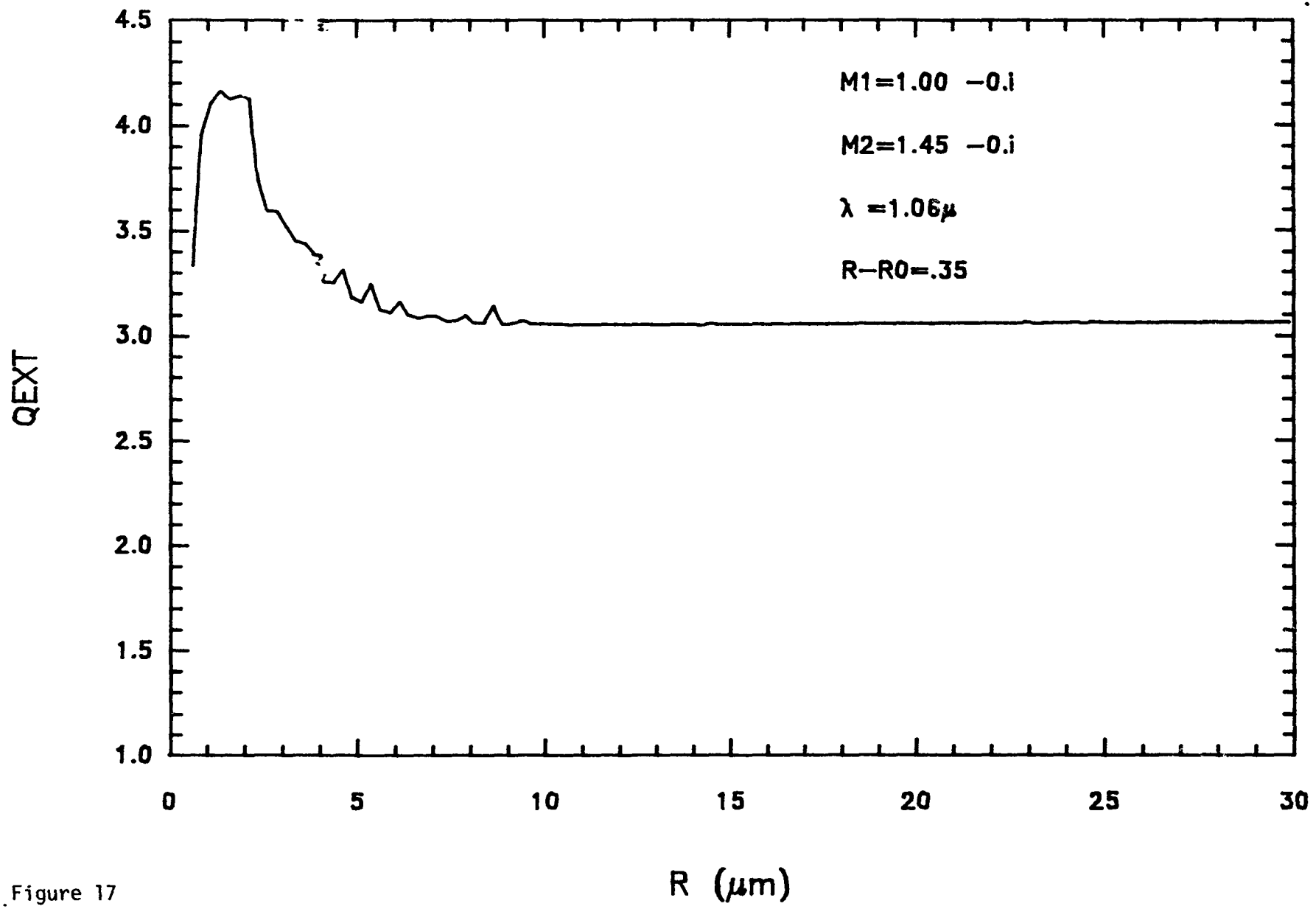
M1=1.00 −0.i
M2=1.45 −0.i
λ =1.06μ
R−R0=.35
QEXT
4.5
4.0
3.5
3.0
2.5
2.0
1.5
1.0
0
5
10
15
20
25
30
R (μm)

Figure 17

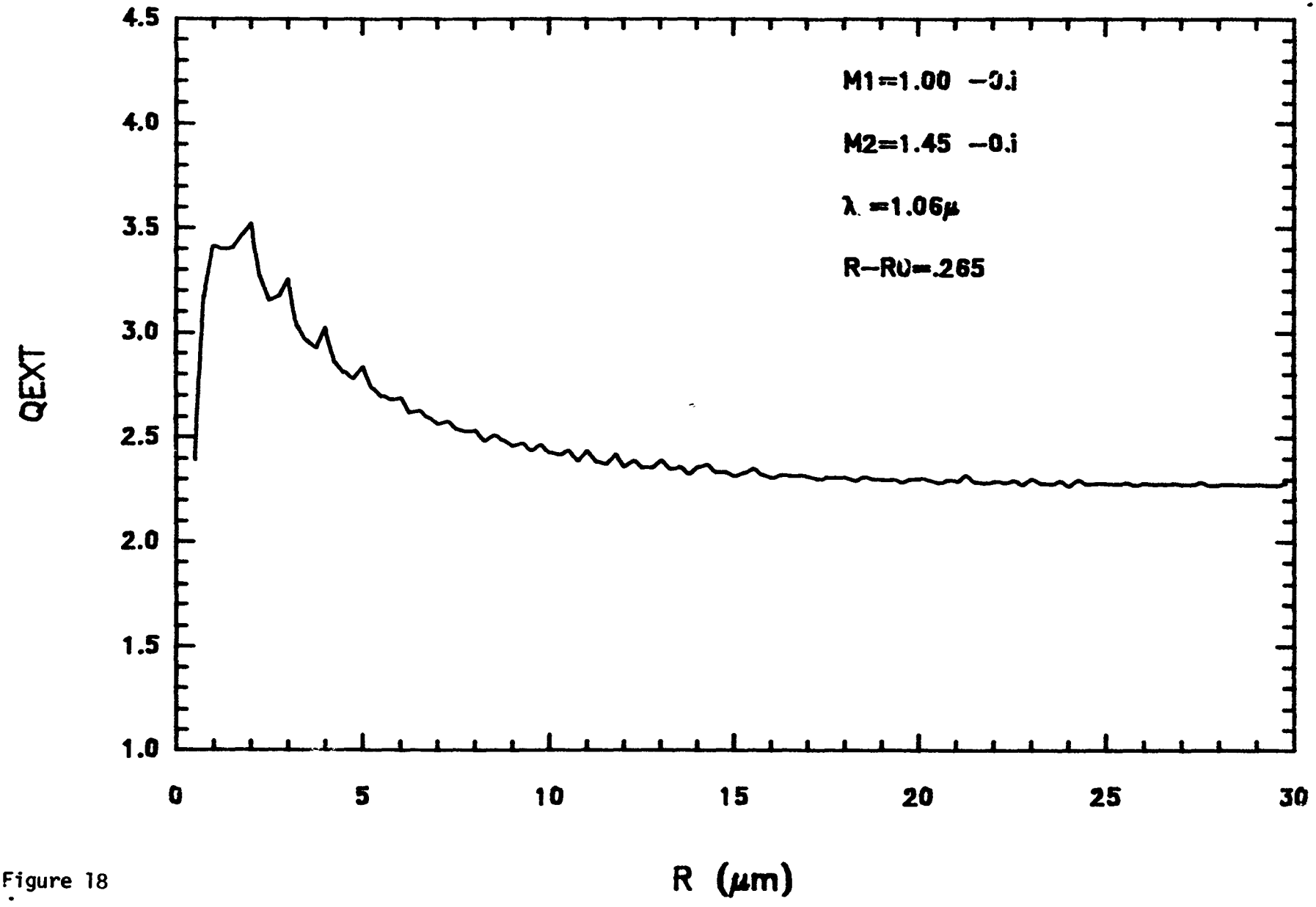
M1=1.00 -0.i
M2=1.45 -0.i
λ =1.06μ
R--R0=.265
QEXT
4.5
4.0
3.5
3.0
2.5
2.0
1.5
1.0
0
5
10
15
20
25
30
R (μm)

Figure 18

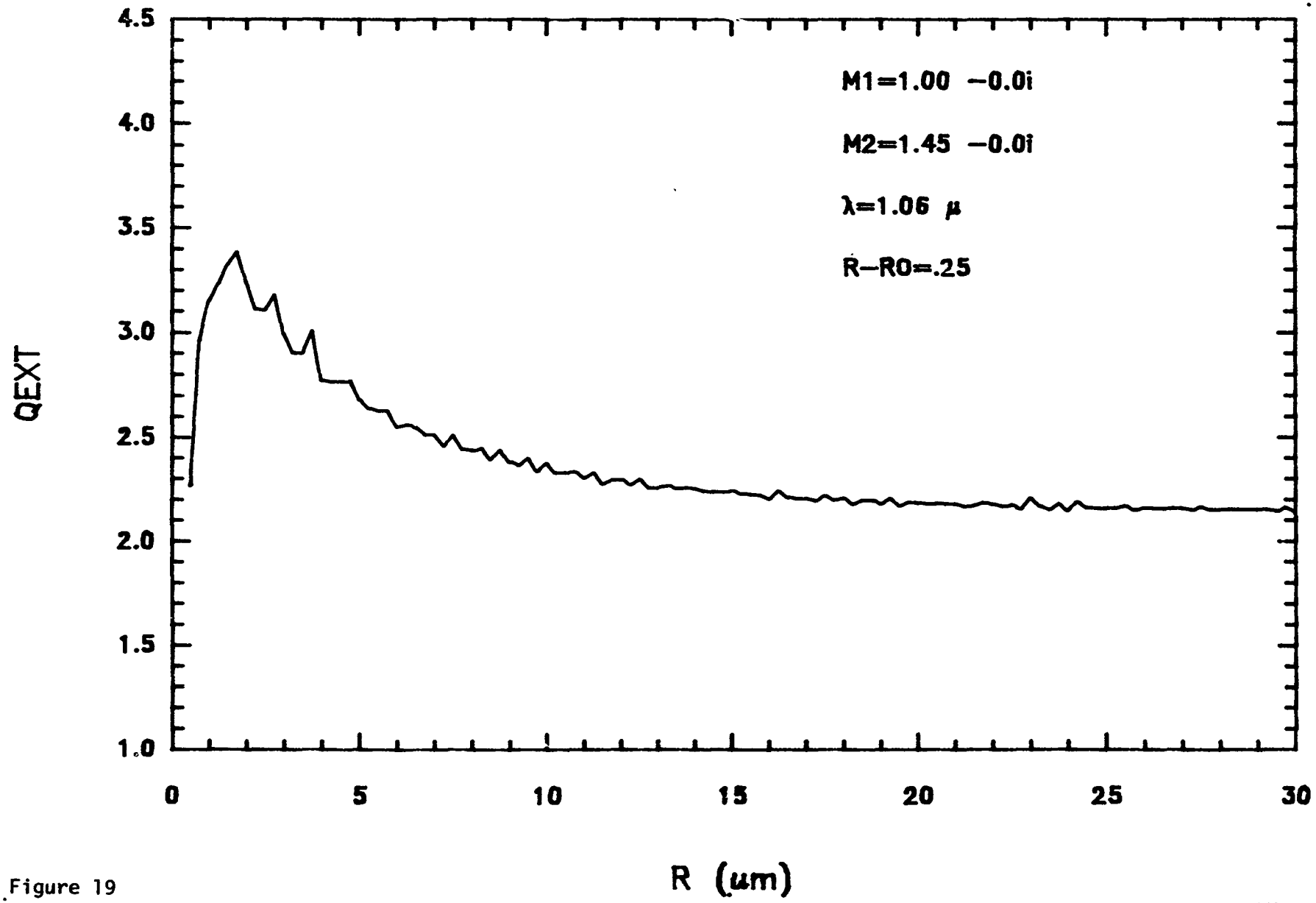
4.5
4.0
3.5
3.0
2.5
2.0
1.5
1.0
QEXT
M1=1.00 −0.0i
M2=1.45 −0.0i
λ=1.06 μ
R−RO=.25
0
5
10
15
20
25
30
R (μm)

Figure 19

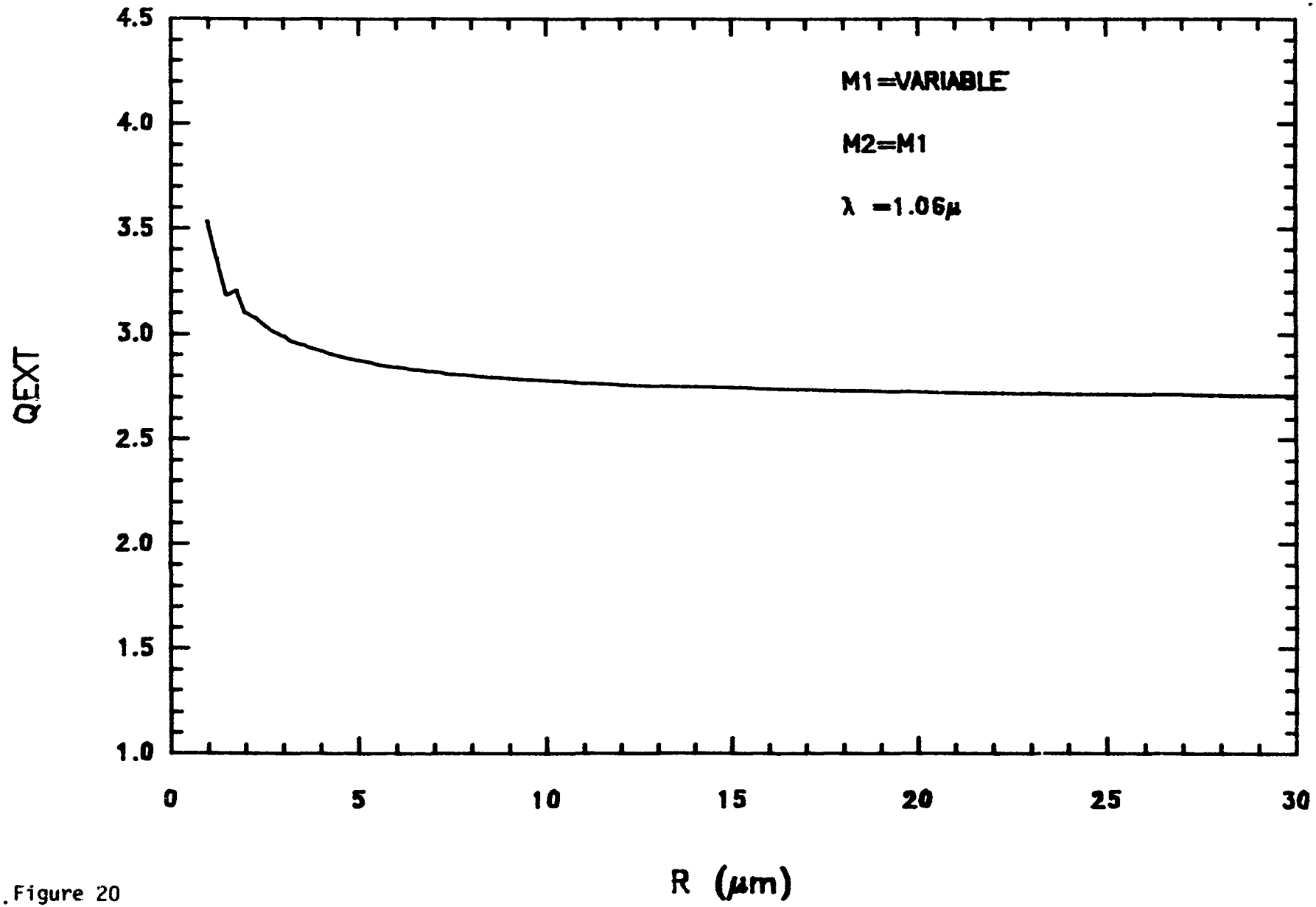
M1=VARIABLE
M2=M1
λ =1.06μ
QEXT
4.5
4.0
3.5
3.0
2.5
2.0
1.5
1.0
0
5
10
15
20
25
30
R (μm)

Figure 20

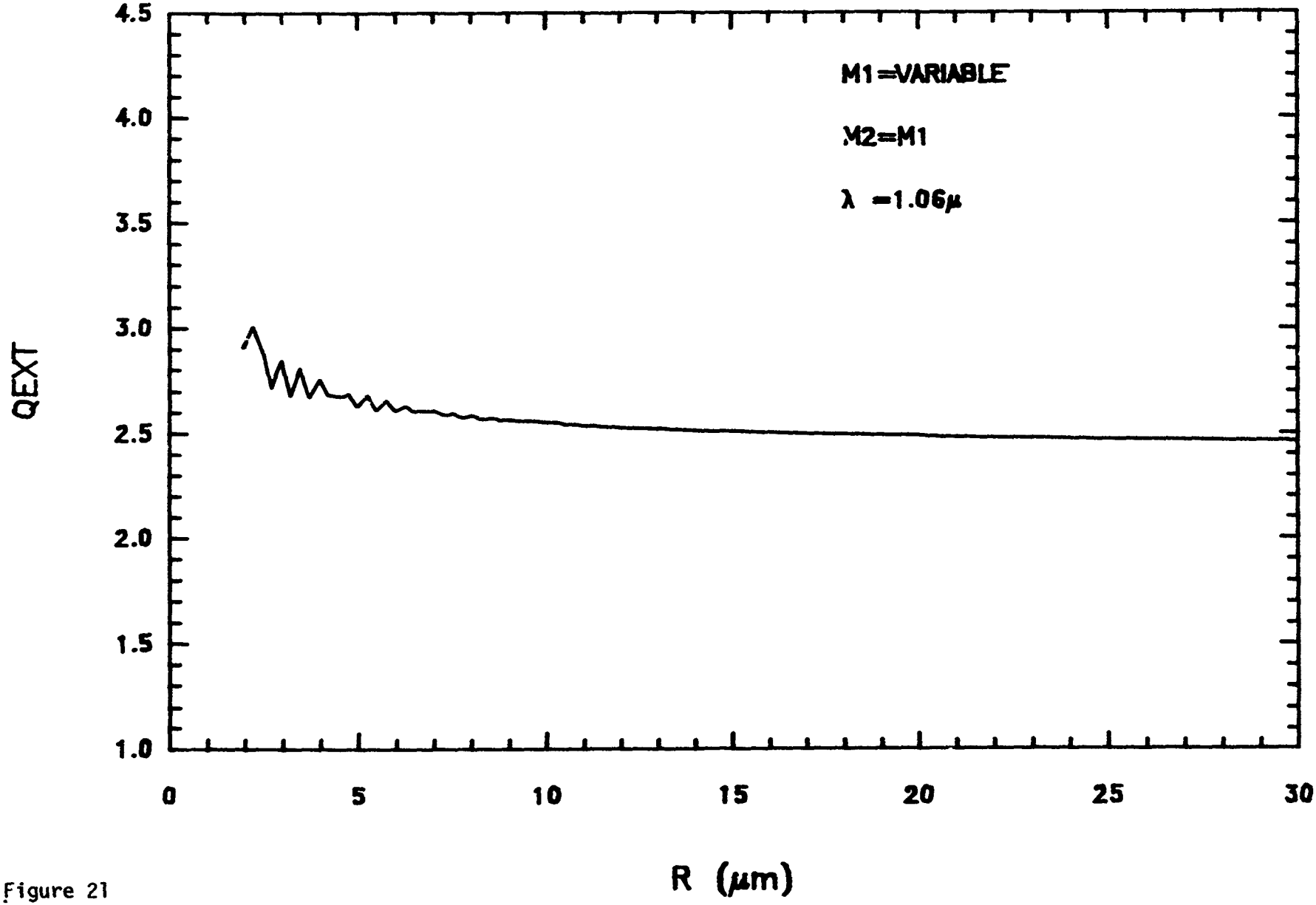
M1=VARIABLE
M2=M1
λ =1.06μ
QEXT
4.5
4.0
3.5
3.0
2.5
2.0
1.5
1.0
0
5
10
15
20
25
30
R (μm)

Figure 21

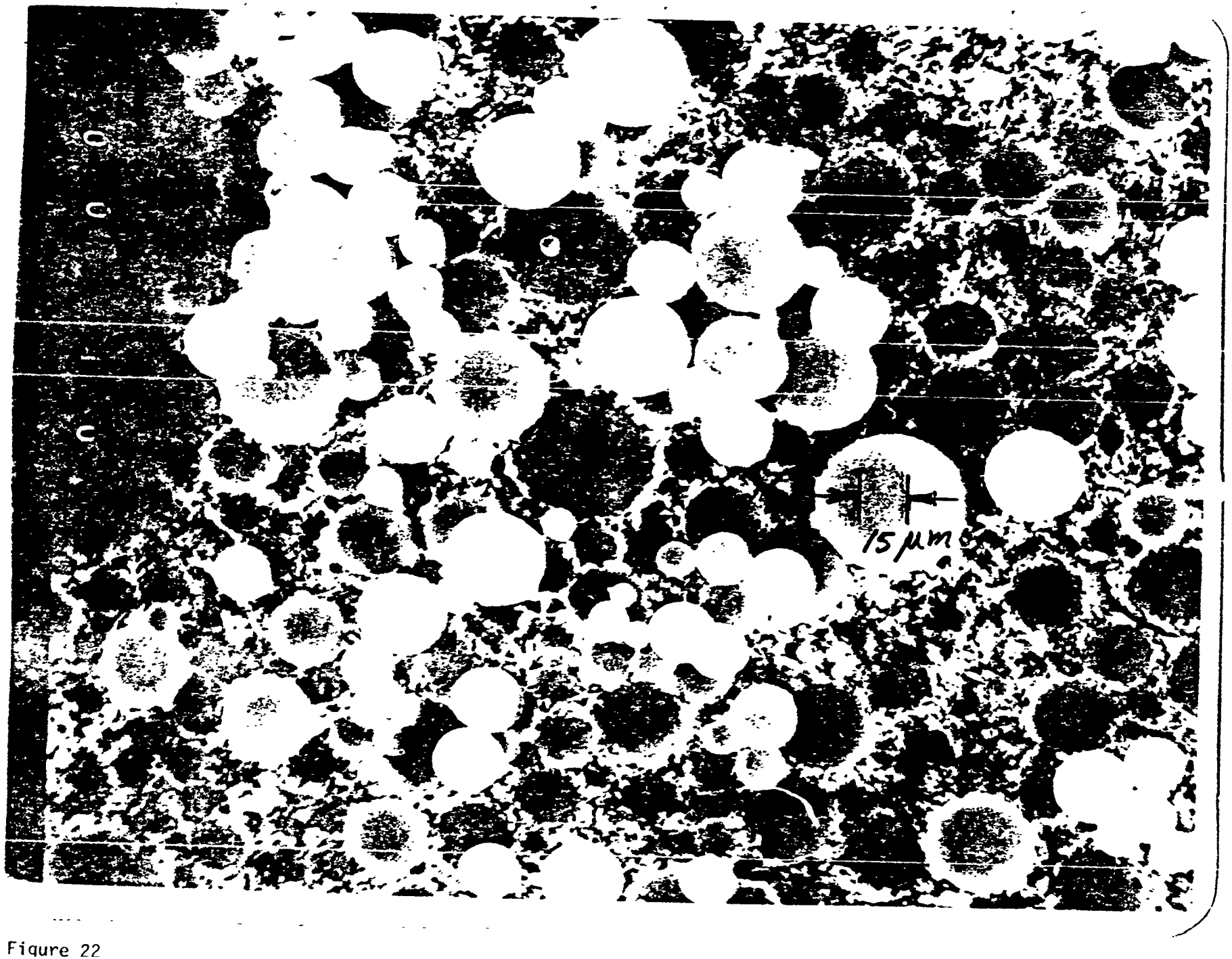

Figure 22

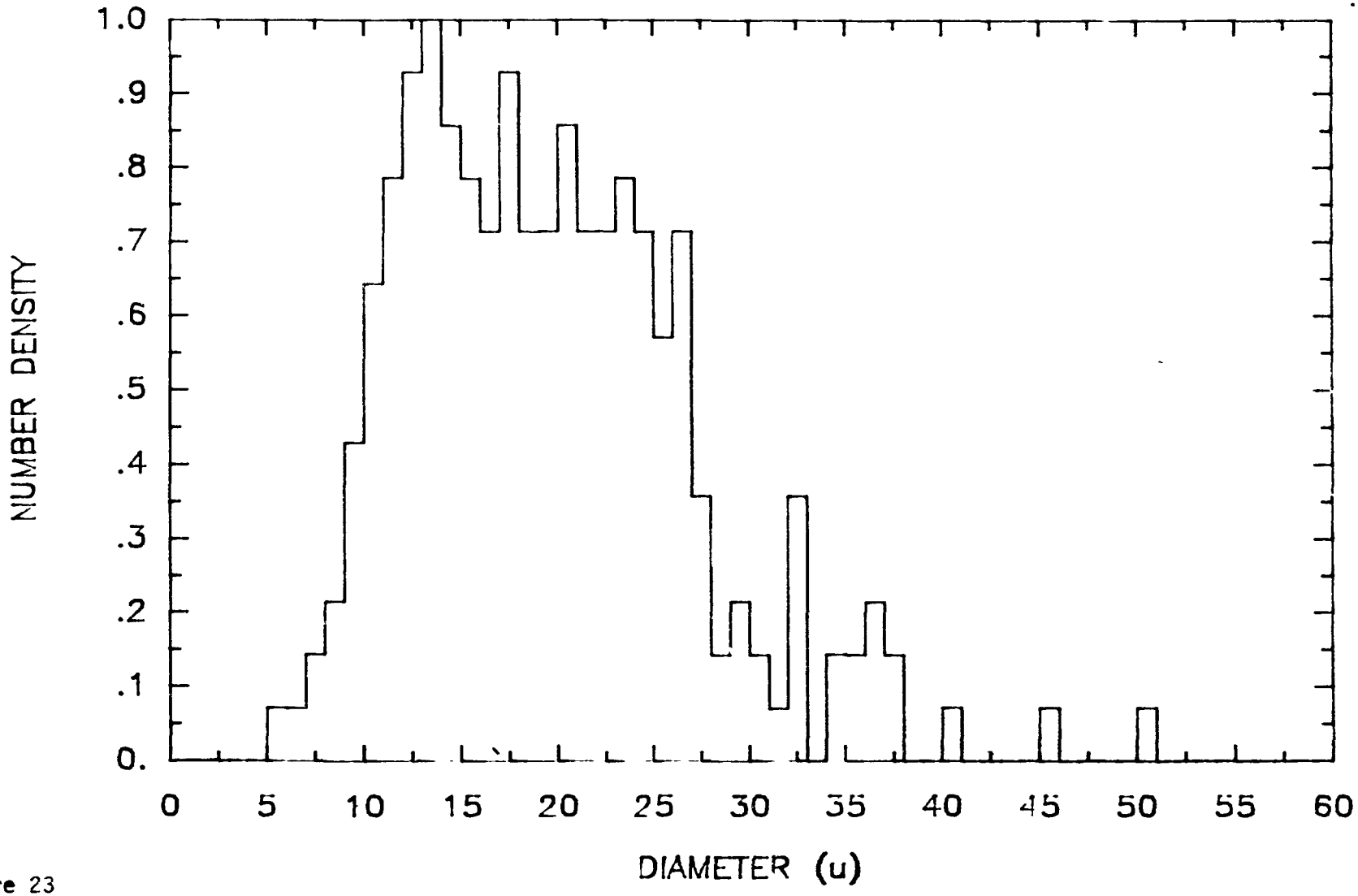
NUMBER DENSITY
1.0
.9
.8
.7
.6
.5
.4
.3
.2
.1
0.
0
5
10
15
20
25
30
35
40
45
50
55
60
DIAMETER (u)

Figure 23

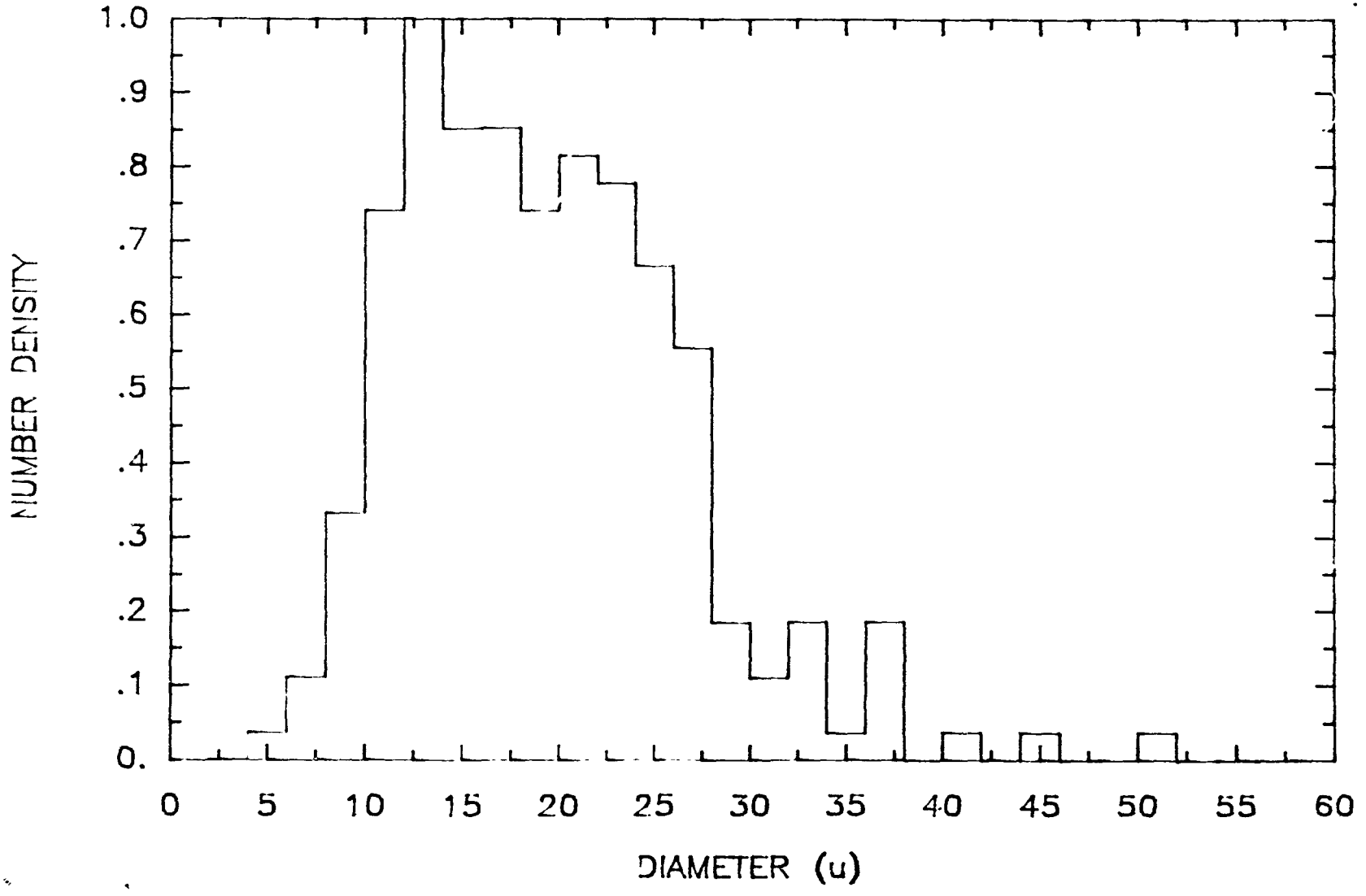
1.0
.9
.8
.7
.6
.5
.4
.3
.2
.1
0.
NUMBER DENISITY
0
5
10
15
20
25
30
35
40
45
50
55
60
DIAMETER (u)

Figure 24

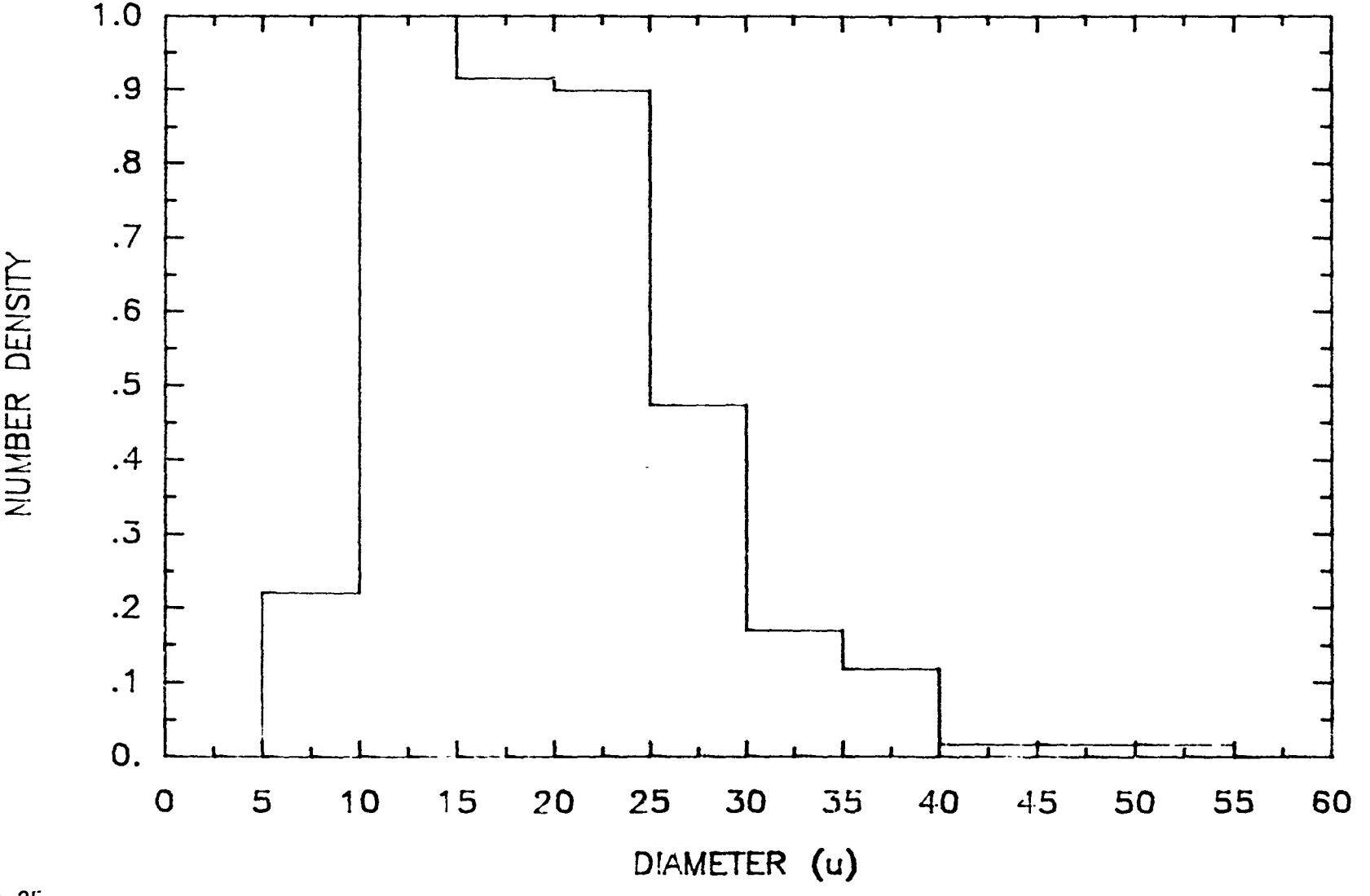
1.0
.9
.8
.7
.6
.5
.4
.3
.2
.1
0.
NUMBER DENSITY
0
5
10
15
20
25
30
35
40
45
50
55
60
DIAMETER (u)

Figure 25

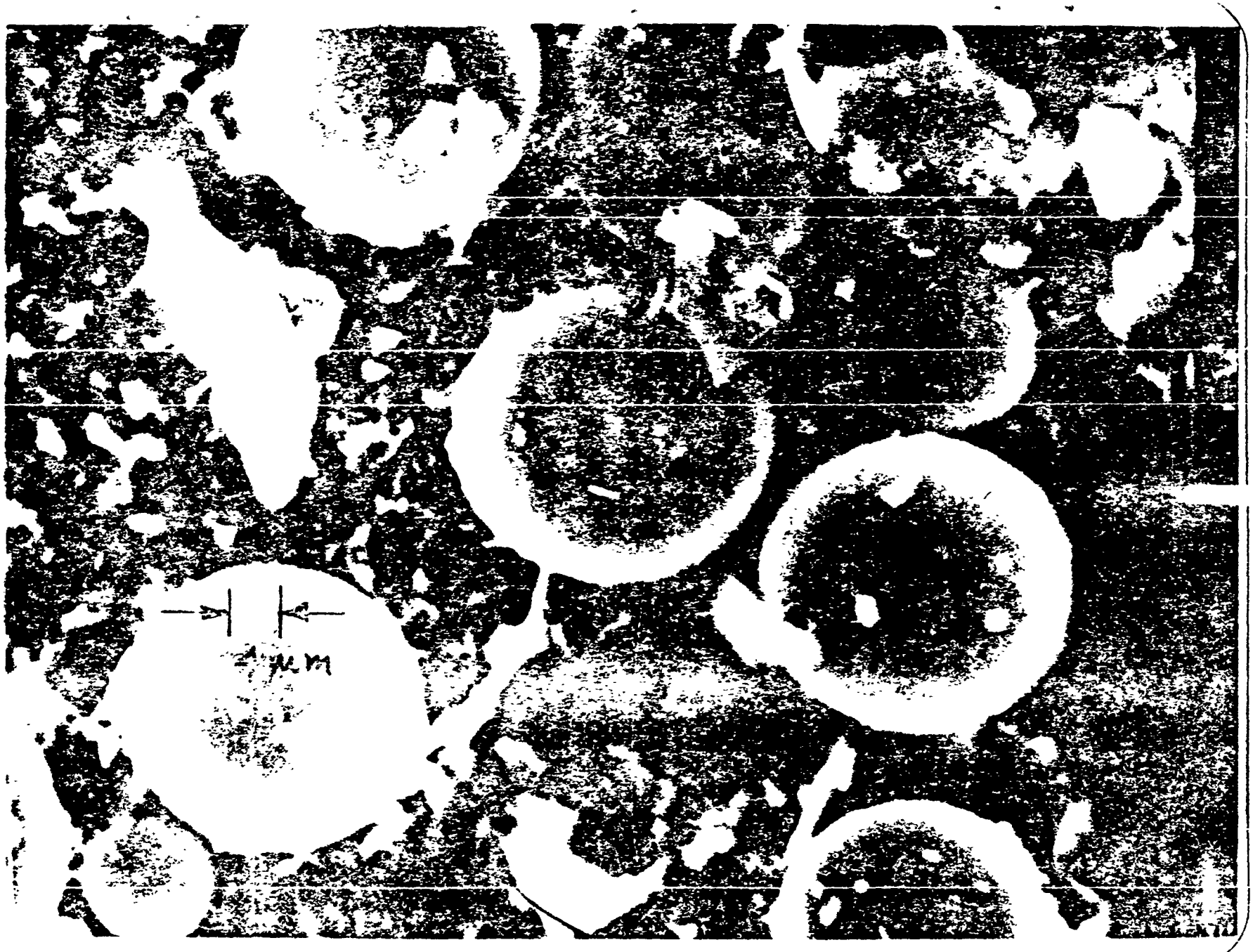

Figure 26